https://doi.org/10.5194/gmd-2020-316
Preprint. Discussion started: 28 October 2020

Geoscientific Model Development Discussions
Open Access

InundatEd: A Large-scale Flood Risk Modeling System on a Big-data - Discrete Global Grid System Framework

Chiranjib Chaudhuri[1], Annie Gray[1], and Colin Robertson[1]

[1]Wilfrid Laurier University, Department of Geography and Environmental Studies, Waterloo, Canada

Email: chiranjibchaudhuri@gmail.com

Keywords: Flood modeling system, Height Above Nearest Drainage, Discrete Global Grid System, IDEAS, Web-GIS, R/Shiny, Manning's Equation, Regional Regression.

https://doi.org/10.5194/gmd-2020-316
Preprint. Discussion started: 28 October 2020

Geoscientific Model Development Discussions

Abstract

Despite the high historical losses attributed to flood events, Canadian flood mitigation efforts have been hindered by a dearth of current, accessible flood extent/risk models and maps. Such resources often entail large datasets and high computational requirements. This study presents a novel, computationally efficient flood inundation modelling framework ("InundatEd") using the height above nearest drainage-based solution for Manning's equation, implemented in a big-data discrete global grid systems-based architecture with a web-GIS platform. Specifically, this study aimed to develop, present, and validate InundatEd through binary classification comparisons to known flood extents. The framework is divided into multiple swappable modules including: GIS pre-processing; regional regression; inundation model; and web-GIS visualization. Extent testing and processing speed results indicate the value of a DGGS-based architecture alongside a simple conceptual inundation model and a dynamic user interface.

https://doi.org/10.5194/gmd-2020-316
Preprint. Discussion started: 28 October 2020

Geoscientific Model Development Discussions
Open Access

Introduction:

Globally from 1994 to 2013 flood events accounted for 43% of recorded natural disasters (Centre for Research on the Epidemiology of Disasters, 2016). Flooding is responsible for one third of natural disaster costs in Europe (Albano, Sole, Adamowski, Perrone, & Inam, 2018), while in Canada mean annual losses of $1-2 billion (CAD) are attributed to flood disasters (Oubennaceur et al., 2019). A 2013 flood in southern Alberta, costing over 1.7 billion dollars (CAD) in insured property damages, is the most expensive natural disaster in Canadian history (Stevens & Hanschka, 2014). Rapid economic development and urbanization during the last few decades – particularly urban development in close proximity to Canadian waters following population expansions of the 1950s-1960s – have increased the amount of exposure and in-turn the economic damages of flood events (Robert et al., 2003). Despite increasing risks and impacts of flood events, many continue to settle in flood-prone areas, making the availability of accurate, timely, and detailed flood information a critical information need (Pal, 2002).

Mitigating the considerable economic impact of flood events; the design of effective emergency response measures; the sustainable management of watersheds and water resources; and flood risk management, including the process of public flood risk education, have long been informed by the practice of flood (inundation) modelling, which aims to understand, quantify, and represent the characteristics and impacts of flood events across a range of spatial and temporal scales (Handmer, 1980; Stevens & Hanschka, 2014; Teng et al., 2017, 2019; Towe et al., 2020). Flood inundation modelling research has increased in response to such factors as predicted climate change impacts (Wilby & Keenan, 2012) and advancements in computer, GIS (Geographic Information Systems), and remote sensing technologies, among others (Kalyanapu, Shankar, Pardyjak, Judi, & Burian, 2011; Vojtek & Vojteková, 2016; Wang & Cheng, 2007). Flood modelling approaches can be broadly divided into three model classes: empirical; hydrodynamic; and simplified/conceptual. Empirical methods entail direct observation through methods such as remote sensing, measurements, and surveying, and have since evolved into statistical methods informed by fitting relationships to empirical data. Hydrodynamic models, incorporating three subclasses (one-dimensional, two-dimensional, and three-dimensional), consider fluid motion in terms of physical laws to derive and solve equations. The third model class, simple conceptual, has become increasingly well-known in the contexts of large study areas, data scarcity, and/or stochastic modeling and encompasses the majority of recent developments in inundation modelling

https://doi.org/10.5194/gmd-2020-316
Preprint. Discussion started: 28 October 2020

Geoscientific Model Development
Discussions

practices. Relative to the typically complex hydrodynamic model class, simple conceptual models simplify the physical processes and are characterized by much shorter processing times (Oubennaceur et al., 2019; Teng et al., 2017, 2019). While each class has contributed substantially to the advancement of flood risk mapping and forecasting practices, a consistent barrier has been the trade-off between computer processing time and model complexity (Neal, Dunne, Sampson, Smith, & Bates, 2018), especially with respect to two-dimensional and three-dimensional hydrodynamic models, which entail specialized expertise to derive and apply physical and fluid motion laws, require adequate data to resolve equations, and the computational resources to process the equations. Neal et al. (2018) summarized the proposed solutions to such challenges as relating to 1) modifications to governing equations or 2) code parallelization, with the latter informing the method proposed in Oubennaceur et al. (2019). With respect to 2D/3D hydrodynamic model code parallelization, Vacondio et al. (2017) listed two approaches: classical (Message Passing Interface) and Graphics Processing Units (GPUs). The GPU-accelerated method has been shown to decrease execution times, whilst avoiding the use of supercomputers, for high-resolution, regional-scale flood simulations (e.g., Ferrari et al. (2020), Vacondio et al. (2017), Wang & Yang (2020), and Xing et al. (2019)). However, the GPU-accelerated method is still limited in terms of the hardware requirement (graphics cards), the use of uniform and/or non-uniform grids (Vacondio et al. (2017)), and the need for specific, specialized modelling programs to handle the input data required to solve complex hydrodynamic equations. The ongoing development of simple conceptual inundation models offers another avenue to handle limitations such as computation requirements and data scarcity, allowing areas poorly served by standard hydrodynamic modeling, to be provided with up-to-date flood extent maps and provided with platforms with which the public can view and interact with the simulated floods (Tavares da Costa, 2019). Although simple conceptual models using such methods as linear binary classification and Geomorphic Flood Index (Samela et al., 2017, 2018) have been, and continue to be, developed, the combination of simple conceptual flood methods with big-data approaches remains largely uninvestigated (Tavares da Costa, 2019).

Recent advances in big data architectures may hold potential to retain enough model complexity to be useful while providing computational speedups that support widespread and system agnostic model development and deployment. There is an increasing need for examination of the potential of decision-making through data-driven approach in flood risk management and investigation a suitable software architecture and associated cohort of methodologies which involves more data-centric architecture (Towe et al., 2020). Discrete global grid systems (DGGS) are emerging as a data model for a digital earth framework (Craglia et al. 2012; Craglia et al., 2008). One of the more promising aspects of DGGS data models to handle big spatial data is their ability to integrate heterogeneous spatial data into a common spatial fabric. This structure is suitable for rapid model developments where models can be split into unit processing regions. Furthermore, with the help of DGGS the model can be ported to a decentralized big-data processing system and many computations can be scaled for millions of unit regions. A recently developed DGGS-based data model and modelling environment called an Integrated Discrete Environmental Analytics System (IDEAS) is one such system which implements a multi-resolution hexagon tiling data structure within a hybrid relational database environment (Robertson, Chaudhuri, Hojati, & Roberts, 2020). Notably, and in contrast to previous systems, the only special installation entailed by IDEAS is a relational database. The system exploits the hardware capability of the database itself which can potentially incorporate the following: GPU(s), distributed storage, and a cloud database. In this paper we employ the IDEAS framework for the efficient computation, simulation, analysis, and mapping of flood events for risk mitigation in a Canadian context.

In Canada, nationwide flood mapping efforts were catalyzed by extensive flood damages to southern Ontario due to Hurricane Hazel in 1954, resulting in the Canadian government's institution of the National Flood Damage Reduction Program (NFDRP) in 1975 (Burrell & Keefe, 1989). The NFDRP, a joint federal/provincial undertaking, entailed a number of co-signed agreements related to the reduction of risks of human suffering, loss of life, of assistance costs, and the limitation of flood mitigation infrastructure (Robert et al., 2003). The program set the stage for the creation of high quality flood risk maps as a medium to provide information to the public, to inform land use zoning, and to inform disaster response strategies, among other goals (Handmer, 1980), and demonstrated the need for and value of effective Canadian flood mapping practices. Regrettably, the program was slowly phased out and terminated by 1996 (Pal, 2002). Flood mapping responsibilities previously encompassed by the program were delegated to various levels of government, resulting in a heterogeneous set of mapping standards and practices which still hinder Canadian flood management practices today (Calamai & Minano, 2017). Moreover, best practices in flood hazard mapping are rarely made freely available to the Canadian public.

https://doi.org/10.5194/gmd-2020-316
Preprint. Discussion started: 28 October 2020

Flood risk maps as decision support tools can build the capacity of individuals to make informed and sustainable investment and residence decisions in an age of climate concern and environmental change (Albano et al., 2018). The current state of public knowledge of flooding risks is unsatisfactory, with an estimated 94% of 2300 Canadian respondents in highly flood-prone areas lacking awareness of the flood-related risks to themselves and their property, per a 2016 national survey (Calamai & Minano, 2017; Thistlethwaite, Henstra, Brown, & Scott, 2018; Thistlethwaite, Henstra, Peddle, & Scott, 2017). Calls for better transparency and access to reliable flood risk maps and data with which to improve public awareness and understanding of flood risks is in line with a contemporary trend toward more open and reproducible environmental models (Gebetsroither-Geringer, Stollnberger, & Peters-Anders, 2018). There is an opportunity to utilize big data architectures and recent developments in flood inundation modelling and risk assessment technologies to make flood risk information more accessible.

The aim of this paper is threefold: 1) propose a simple conceptual inundation model implemented in big-data architecture; 2) test the model and its results through comparison to known extents of previous flood events; and 3) present the resultant flood maps via an open source, interactive web application.

2. Methods

2.1 Overview

The modelling component of InundatEd incorporated four general stages: 1) GIS pre-processing; 2) flood frequency analysis and regional regression; 3) the application of the catchment integrated Manning's Equation; 4) the application of FEMA's Hazus Depth-Damage functions; and 5) upscaling the model to a discrete global grid systems data model. Sections 2.2.1 to 2.2.5 describe stages 1-5 respectively.

The second component of InundatEd's development was the design of a Web-GIS interface, described in Section 2.3, which liaises with and between the big data architecture, the flood models' outputs as defined by user inputs, and FEMA's Hazus depth-damage functions (Nastev & Todorov, 2013). Section 2.4 subsequently links the Web-GIS interface conceptually to previous sections by providing a summary of InundatEd's system structure and its operation. Finally, simulated flood extents using InundatEd's methodology were compared to the extents of observed, historical flood extent polygons within the Grand River watershed and the Ottawa River watershed, provided respectively by the Grand River Conservation Authority and Environment Canada. The comparison and testing process is described in Section 2.5.

2.2. Modelling

2.2.1 – Stage 1: GIS Pre-processing

The following GIS input data were obtained from Natural Resources Canada for the Grand River and Ottawa River watersheds and cropped to their respective study area: Digital Elevation Models (Canada Centre for Mapping and Earth Observation, 2015); river network vector shapefiles (Strategic Policy and Innovation Centre, 2019); and Land Use Land Cover (LULC) (Canada Centre for Remote Sensing, 2019). Figure 1 shows the input Digital Elevation Model data, with elevation values given in metres with reference to the CGVD2013 vertical datum. The remaining GIS input data is shown in Supplementary Figure S1. Very small networks, independent of the higher-order channels, were deleted from both regions. ArcGIS Desktop's Raster Calculator tool was used to burn the river network vector into the DEM in preparation for further analysis. TauDEM (Terrain Analysis Using Digital Elevation Models) (Tarboton, 2005), an open-source tool for hydrological terrain analysis, was then used to determine drainage directions and drainage accumulation (Tarboton & Ames, 2004) within the watersheds of interest. Each watershed's drainage network was then established in TauDEM by defining a minimum threshold of two square kilometres on the contributory area of each pixel for the Grand River watershed and ten square kilometres for the Ottawa River watershed. Separately, a value of Manning's n was determined for each 30 x 30 metre pixel of the study areas based on land use/ land cover attributes (Comber & Wulder, 2019). To this end, the input LULC classes (Canada Centre for Remote Sensing, 2019) within the study watersheds were mapped to the nearest class of the similar land cover classes documented in Chow (1959, Table 5-6) and Brunner (2016, Figure 3-19), from which the respective values of Manning's N were used. Table 1 provides the utilized input LULC classes, their respective description provided by NRCAN, and the employed n values. Height Above Nearest Drainage (HAND) (Rahmati, Kornejady, Samadi, Nobre, & Melesse, 2018; Garousi-Nejad, Tarboton, Aboutalebi, & Torres-Rua, 2019) was also calculated in TauDEM with reference

https://doi.org/10.5194/gmd-2020-316
Preprint. Discussion started: 28 October 2020

to the DEM and derived drainage network. Figure 2 provides a visual accounting of this stage of the modelling component.

2.2.2. Stage 2: Regional Regression and Flood Frequency Analysis

The index flood approach - a regional regression model based on annual maximum discharge data (Darlymple, 1960) and described in Hailegeorgis & Alfredsen (2017)- was used to derive the discharges by return period at sub-catchment outlets. The model includes two sections: a) a relationship between index flood and contributory upstream area for each hydrometric station and each subcatchment outlet (regional regression); and b) a flood frequency analysis to estimate the quantile values of the departures,with a departure defined as discharge at given station divided by the index flood of that same station). The index flood approach entails the following assumptions: a) the flood quantiles at any hydrometric site can be segregated into two components – an index flood and regional growth curve (RGC) -; b) the index flood at a given location relates to the (sub)catchment characteristics via a power-scaling equation, either in a simpler case which considers only upstream contributory area or in a more complex case which incorporates land use/ land cover, soil, and climate information; and c) within a homogeneous region the departure/ratio between the index flood and discharge at hydrometric sites yields a single regional growth curve which can relate the discharge and return period.

Per assumption a, the index flood at each hydrometric station is required. To this end, annual maximum discharge values (m^3s^{-1}) were extracted within R (R Core Team, 2019) at hydrometric stations maintained by Environment Canada within the Grand River and Ottawa River watersheds (HYDAT) (Hutchinson, 2016). Only stations with a period of record >= 10 years of annual maximum discharge were maintained (n = 32 and n = 54, respectively). The minimum and maximum periods of record for the Grand River watershed were 12 years and 86 years, respectively. Periods of record for the Ottawa River watershed ranged from a minimum of 10 years to a maximum of 58 years. A median annual maximum discharge value was then calculated ($\tilde{Q}$) for each hydrometric station. As discussed in Hailegeorgis & Alfredsen (2017), although the index flood is generally the sample mean of a set of annual maximum discharge values, index floods have also been evaluated based on the sample median (eg. Wilson et al., 2011) at the suggestion of Robson & Reed (1999). Finally, the index flood values ($\tilde{Q}$) were used to normalize the observed annual maximum discharge values (Q) at their respective station ($q_i = Q/\tilde{Q}$).

https://doi.org/10.5194/gmd-2020-316
Preprint. Discussion started: 28 October 2020

With respect to regional regression and assumption b of the index flood method, a generalized linear model was applied to relate $\log_{10}$ transformed Q̃ values to $\log_{10}$ transformed upstream area values at each hydrometric station. The generalized linear model assumed an ordinary least squares error distribution. The results of the generalized linear model for each watershed allowed for the calculation of previously unknown Q̃ values for each subcatchment outlet. In a more complex model (Fouad et. al. 2016), other catchment characteristics such as land use/land cover, geology, etc. could be used. However, in the case of the proposed model the correlations between the calculated and observed index floods, on the sole basis of discharge records and a linear model relating upstream area, were high as discussed in the Results section. Thus, the simpler method was used to estimate index floods and to relate index flood to contributory area at hydrometric stations and subcatchment outlets. Thus, the regional regression model derived a relationship between index flood (Q̃) and upstream contributory area for each hydrometric station i or subcatchment outlet. The relationship between index flood at station i or at a subcatchment outlet ($\widetilde{Q^{\iota}}$) and upstream contributory area (A_i) is given by:

$$\tilde{Q}^i = aA_i^c \quad (1)$$

where a is the index flood discharge response at a unit catchment outlet (or at a hydrometric station) and c is the scaling constant. We took the logarithm of Equation (1) on both sides - a procedure used in noted in Hailegeorgis & Alfredsen (2017) as used in Eaton, Church, & Ham (2002) - yielding a linear relationship which was solved using the Ordinary Least Squares approach (Haddad et al. (2011).

The selection of a suitable probability distribution model – a common tool in hydrologic modelling studies (Langat et al., 2019; Singh, 2015)- for use in a watershed where the flow has been modelled due to human abstraction is a fundamental step of the analysis process and must account for disturbance-related changes to the extreme value characteristics of the flow. While solutions to this problem have been proposed in the literature, artificial abstraction fundamentally changes the extreme value characteristics of the flow, thereby hindering the usability of most distributional forms (Kamal et. al. 2017). Many researchers have tried to address this problem by putting explicit assumptions on types of non-stationarity affecting the river discharge and are able to devise a closed mathematical formulation which enables the parametric distributions to handle such non-stationarity. However, such methods typically entail knowledge of the specific design return periods of individual flood prevention structures (Salas & Obeysekera, 2014), many of which are absent in our case. To circumvent this problem, we used a non-parametric approach for the regional growth curve (RGC), which requires no fundamental sample characteristics. Thus, modified flood records and limited information notwithstanding, flood frequency estimation is possible using the index flood approach. Per assumption c of the index flood method, a log-spline non-parametric approach was taken to model a RGC (Stone, Hansen, Kooperberg, & Truong, 1997) for each study watershed. Specifically, the index flood values ($\tilde{Q}$) were used to normalize the observed annual maximum discharge values (Q) at their respective station ($Q_i = Q/\tilde{Q}$). The Q_i values (n= 1487 and n = 1248 for the Ottawa River watershed and the Grand River watershed, respectively) were then fitted to a logspline distribution for their respective watershed. The discharge quantiles (Q_r) were extracted for the following return periods (T, years): 1.25, 1.5, 2.0, 2.33, 5, 10, 25, 50, 100, 200, and 500. The return periods were first converted to a cumulative distribution function:

$$\text{CDF} = 1 - \left(\frac{1}{T}\right) \quad (2)$$

Finally, flood quantile estimations were calculated for each return period as shown below:

$$Q_T^i = \widetilde{Q^i} q_T \quad (3)$$

such that T is a specified return period in years; Q_T^i is a quantile estimate of discharge for the specified return period T (years) at a specified station i (or a subcatchment outlet); $\widetilde{Q^i}$ is the "index flood" at the same station i (or at the same subcatchment outlet); i = 1,2,…,N where N =32 for the Grand River watershed or N= 54 for the Ottawa River watershed; and q_T is the regional growth curve as described above. Figure 3 provides a visual accounting of the regional regression and flood frequency analysis methodology described in this section.

2.2.3 Stage 3: Catchment Integrated Manning's Equation

Manning's formula (Song et. al., 2017) is widely used to calculate the velocity and subsequently the discharge of any cross-section of an open channel. The Manning's equation is given in SI units by:

$$Q = \frac{1}{n} R_h^{\frac{2}{3}} A\, S^{\frac{1}{2}} \quad (4)$$

such that Q is discharge in cubic metres per second, A represents the cross-sectional area, n is a roughness coefficient, R_h is the hydraulic radius, and S represents slope (fall over run) along the flow path. Despite its widespread use, robustness, and relative ease of use, Manning's Equation has an inherent problem which comes from the uncertain orientation of cross-sections. To mitigate this problem, we integrated Manning's Equation along the drainage lines within the catchment,

https://doi.org/10.5194/gmd-2020-316
Preprint. Discussion started: 28 October 2020

Geoscientific Model Development Discussions

accounting for the slope of each grid cell to yield bed area and derived the stage-discharge relationship. This strategy uses hydrological terrain analysis, discussed previously in Section 2.2.1, to determine the Height Above Nearest Drainage (HAND) of each pixel (Rodda, 2005; Rennó et al., 2008). The HAND method determines the height of every grid cell to the closest stream cell it drains to. In other words, each grid cell's HAND estimation is the water height at which that cell is immersed. The inundation extent of a given water level, can be controlled by choosing all the cells with a HAND less than or equal to the given level. The water depth at every cell can then be calculated as the water level minus the HAND value of the corresponding cell. The relevance of HAND to the field of flood modelling has been demonstrated in the literature (Rodda, 2005, Nobre et al., 2016). Its documented use notwithstanding, HAND's potential applications to the depiction of stream geometry information and to the investigation of stage-discharge connections have not been well investigated. Hydraulic methods of discharge calculation typically entail hydraulic parameters derived from the known geometry of a channel. In contrast, the HAND method does not require channel geometry to determine hydraulic parameters.

The conceptual framework for implementing HAND to estimate the channel hydraulic properties and rating curve is as follows: for any reach at water level h, all the cells with a HAND value < h compose the inundated zone F(h), which is a subarea of the reach catchment. The water depth at any cell in the inundated zone F(h) is the difference between the reach-average water level h and the HAND of that cell, $HAND_c$, which can be represented as: depth = $HAND_c$-h. Since a uniform reach-average water level h is applied to check the inundation of any cell within the catchment, the inundated zone F(h) refers to that reach level. The water surface area of any inundated cell is equal to the area of the cell A_c. This case study uses 30 metre x 30 metre grid cells, thus in this case $A_c = 900\ m^2$. The channel bed area for each inundated cell is given by

$$A_s = A_c\sqrt{(1 + slope^2)} \quad (5)$$

where slope is the surface slope of the inundated pixel expressed as rise over run or inverse tangent of the slope angle. This equation approximates the surface area of the grid cell as the area of the planar surface with surface slope, which intersects with the horizontal projected area of the grid cell. The flood volume of each inundated pixel at a water depth of h can be calculated as V_c (h)=A_c (h-$HAND_c$). If the reach length L is known, the reach-averaged cross section area for each pixel is given by A_i=V_c/L. Similarly, the reach-averaged cross section wetted perimeter for each inundated

https://doi.org/10.5194/gmd-2020-316
Preprint. Discussion started: 28 October 2020

pixel $P_i(h)= A_s/L$. Therefore, the hydraulic radius for each inundated pixel is given by $R_i=A_i/P_i$. Therefore, we can estimate the reach-averaged cross-section area $A = \sum_i A_i$, perimeter $P = \sum_i P_i$, and hydraulic radius $R= A/P$ for the entire flooded area. The composite Manning's n is estimated using the Lotter method (Tullis, 2012) and is given by:

$$n = \frac{PR^{\frac{5}{3}}}{\sum_i \frac{1}{n_i} P_i R_i^{\frac{5}{3}}} \quad (6)$$

Thus the discharge Q(h) corresponding to inundation height can be computed by the Manning's equation and given by:

$$Q(h) = \frac{1}{n} R^{\frac{2}{3}} A S^{\frac{1}{2}} \quad (7)$$

where S is the slope of the river. Figure 4 displays the sequence of methods outlined for the Catchment Integrated Manning's Equation method.

<u>2.2.4 Stage 4: Damage Computation</u>

To contextualize the modelled inundation depths, FEMA's Hazus Depth-Damage functions were applied to the calculated depths via the R package Hazus (https://www.fema.gov/hazus) (Goteti, 2014). Using the Hazus package, estimated percentage losses can be generated for model output inundation depths at individual locations specified by the user. Furthermore, the Hazus loss percentages are contingent on building-specific properties, offering a built-in variety of building types, descriptions, and situations (e.g., fresh water vs. salt water) to tailor final estimations to a user's personal experience. The use of Hazus within the R Development environment allows for seamless integration with a user interface for inputs such as building type.

<u>2.2.5 Stage 5: Upscaling and Data Conversion</u>

The proposed InundatEd inundation model simulates the flood-depth distributions for each catchment independently. This makes this model suitable to be ported to a DGGS-based data model and processing system. Following the GIS preprocessing, done in TauDEM as discussed in Section 2.2.1, the required data was converted to a DGGS representation, as outlined in Robertson et al., (2020). Supplementary Figure S2 for raster input data (S2a), polygon (vector) input data (S2b), and network (directional polyline vector) input data (S2c). For raster data (S2a), the bounding box is used to extract a set of DGGS cells, and then for each DGGS cell's centroid the

https://doi.org/10.5194/gmd-2020-316
Preprint. Discussion started: 28 October 2020

raster value is extracted. To convert polygon data to a DGGS data model, we sample from its interior and its boundary separately using uniform sampling. Then each sample point is converted into DGGS cells based on its coordinates and stored into IDEAS data model by aggregating both sets of DGGS cells (Figure S2b). The same process for the border extraction is applied to the polylines and networks, however with network data the order of the cells is also stored as a flag to use in directional analysis (Figure S2c). Following conversion, the data was ported to a 40-node IBM Netezza Database for subsequent calculations. General, systematic limitations of the InundatEd IDEAS-based inundation model are discussed in Section 3.1.

2.3 Web-GIS Interface

The R/Shiny platform and the R-Studio development environment were used to design the user interface and server components of an online web application, allowing users to query and interact with the inundation model. Features of R specific to InundatEd's modelling workflow were its support of the Hazus damage functions and its support for DGGS spatial data. Shown in Figure 5a, the InundatEd user interface offers widgets for the following user inputs: address (text); discharge (slider); and return period (dropown), as well as tabs for viewing interactive graphs. The InundatEd user interface also features an interative map which leverages the Leafgl R package (Appelhans & Fay, 2019) for seamless integration with the DGGS data model. Users may click on the map to obtain point-specific depth information, which can be passed to the Hazus damages computation.

2.4 InundatEd Flood Information System – System Structure Summary

Figure 5b displays the overall system structure and linkages for the InundatEd flood information system. GIS input data, as discussed in Section 2.2, were staged, pre-processed, and ported to the database. Data querying was used to compute 'in-database' inundation (flood depth) and related damages (methods outlined in Section 2.1) in response to user interface inputs to the R/Shiny UI.

2.5 Flood Data Comparison and Model Testing

2.5.0 Study Areas

As preliminary testing domains, we created flood inundation models for the Grand River Basin and Ottawa River Basin respectively, both located in Ontario, Canada. Each basin has experienced historical flooding and have implemented varying measures of flood control. Table 2 shows different salient characteristics of these catchments. For the purposes of graphing and discussion of station-specific period of record (number of years with a recorded annual maximum discharge) on theoretical vs estimated flood quantiles, two stations from each study watershed were selected, one each for high period of record and low period of record. For the Grand River watershed, stations 02GA003 and 02GA047 were selected for high and low period of record, respectively. For the Ottawa River watershed, stations 02KF006 and 02JE028 were selected, respectively. "Theoretical quantiles" are here defined as the quantiles generated by our model based on the logspline fit, which incorporates annual maximum discharge values from multiple stations across each study watershed (Section 2.2.2 and Figure 3). In contrast, "estimated quantiles" are here defined as the flood quantiles calculated simply by extracting the quantiles for the desired return periods from the raw annual maximum discharge values observed at the hydrometric station of interest.

2.5.1. Ottawa River Watershed

Four flood extent polygons (FEPs) provided by Natural Resources Canada (Natural Resources Canada, 2018, 2020) from the May-June 2019 flood season were used as "observed" floods to test the model outputs for the Ottawa River watershed. Each FEP represented a previously digitized floodwater extent at a specified date/time.

A second criterion for selection was that the hydrometric station(s) intersected by the FEP provided discharge data for the FEP's respective datetime. Two hydrometric stations which met both criteria were selected: 02KF005 and 02KB001. The following procedure was followed for each FEP using the corresponding hydrometric station (02KF005 or 02KB001), the station level index flood ($\tilde{Q}$, previously calculated during Section 2.2.2), and the observed discharge (Q_{obs}). In both cases, the logspline fit for the Ottawa River watershed, previously generated during Section 2.2.2, was also used.

https://doi.org/10.5194/gmd-2020-316
Preprint. Discussion started: 28 October 2020

Geoscientific Model Development Discussions

The observed discharge (Q_{obs}) was divded by the corresponding hydrometric station's index flood ($\tilde{Q}$) ($Q_i = Q_{obs} / \tilde{Q}$) The cumulative probability of Q_i was converted to a return period using the following equation:

$$\text{return period (years)} = \frac{1}{1-cumulative\ probability} \quad (8)$$

To generate each simluated flood for comparison to its observed counterpart, the methodology outlined in Sections 2.2.2 and 2.2.3 was repeated with the four new return periods appended to the original list of return periods in Section 2.2.2. Table 3 lists each FEP, the corresponding intersected hydrometric station, the period of record used for each station to calculate $\tilde{Q}$, the observed discharge, the resultant cumulative probability value, and the final return period used to generate each simulated flood.

2.5.2. Grand River Watershed

Regulatory floodplain extent data (the greater of RP=100 or discharge from Hurricane Hazel, "observed" flood extent) was obtained from the Grand River Conservation Authority (GRCA) (Grand River Conservation Authority, 2019). However, analysis revealed that, at most hydrometric stations in the Grand River wateshed, the 100-year return period yielded higher discharge values relative to the "Hurricane Hazel" storm. Thus, the 100-year return period could be used. The estimated flood extent for RP=100 was generated per sections 2.2.1-2.2.3. Table S1 provides a discharge comparison between the 100-year return period and the regulatory storm.

2.5.3. Flood Extent Comparisons

For both the Grand River watershed and the Ottawa River watershed, only those subcatchments in close proximity to the observed flood extent polygons were retained for visualization purposes. To this end, a criterion was applied to subcatchments in the Grand River watershed requiring an intersection with the observed flood polygon of >= 20% of the subcatchment's area. For the Ottawa River watershed, due to the use of station-specific observed discharges, an additional criterion was applied: that a given subcatchment intersects with a network line with contributory upstream area >= 80% and contributory upstream area <= 120% of the observed upstream area of the hydrometric station (02KF005 or 02KB001). Table S2 provides by-subcatchment areas of the observed flood extent polygons whose subcatchments were eliminated based on the 20% intersection threshold. Per Table S2, one excluded subcatchment (10505) had an intersection value >= 20%, attributable in part to the presence of a tributary along which it was not expected that the return period would be properly scaled but which intersected the subcatchment. Additionally, due to the pluvial nature of the flooding in that subcatchment, it was once again expected that the return period as a function of the river discharge would not be properly scaled without the presence of a hydrometric station to provide discharge information.

Binary classification metrics have been used to compare between observed and simulated floods in cases where the focus is on extent, not depth (eg Papaioannou et al., 2016; Wing et al., 2017; Chicco & Jurman, 2020). A binary classification (or 2x2 contingency) method was used to compare the simulated flood extent rasters to the extents of their observed counterparts, whereby a confusion matrix was generated for each subcatchment. Multiple accuracy measures were calculated from the contingency tables to support the evaluation of the flood model, including: True Positive Rate (TPR). True Negative Rate (TNR), Accuracy, Matthews Correlation Coefficient (MCC) (Chicco & Jurman, 2020), and the Critical Success Index (CSI) (e.g., Papaioannou et al, 2016; Stephens & Bates, 2015). The MCC is a summary measure of a confusion matrix which is robust to differences in abundance in classes. Matthews Correlation Coefficient (MCC) is defined as:

$$MCC = \frac{TP \ x \ TN - FP \ x \ FN}{\sqrt{(TP+FP)(TP+FN)(TN+FP)(TN+FN)}} \quad (9)$$

Such that TP = true positive, TN = true negative, FP = false positive, and FN = false negative.

3. Results and Discussion

3.1 Model Processes and DGGS

Intermediate model outputs for the Grand River and Ottawa River watersheds - Height Above Nearest Drainage, delineated river networks, and Manning's n- are displayed in Figure 6.

Figure 7 visualizes results for the Grand River watershed and for the Ottawa River watershed for the following method components: calculation of hydrometric station upstream (contributory) area; index flood regression as represented by the correlation of logged index discharge and logged upstream area; and flood frequency as represented by discharge against a Gumbel transformed return period (years), for the stations respectively representative of high and low observations. Figures 7a and 7b plot the log of calculated upstream area against the log of observed upstream area, yielding respective Pearson correlation coefficients of 0.99 and 0.63 for the Grand River and Ottawa River watersheds. The difference in correlation quality can be accounted for in part by the difference in the relative complexities of the delineated networks of the Grand River and Ottawa River watersheds. With respect to regional regression, Figure 7c visualizes the relationship between predicted index flood discharge and contributory upstream area, at individual hydrometric stations, for the Grand River and Ottawa River watersheds (R = 0.83 and 0.95, respectively).The regional growth curves for both the Grand River watershed and the Ottawa River watershed are shown in Figure 7d. To compare the proposed approach of using log-spline distribution against a traditional parametric distribution we fitted a Generalized Extreme Value (GEV) distribution to the RGC (Supplementary Figure S3). With respect to the log-spline RGCs, AIC values of 1861.69 and 867.69 and (-2)(logliklihood) values of 1826.04 and 809.26 were reported for the Grand River watershed and Ottawa River watershed respectively. The log-spline (-2)(logliklihood) values were lower than their GEV counterparts (1837.56 and 880.12) for both watersheds. For the Ottawa River watershed, the log-spline AIC value, 867.69, was also lower than that of its GEV counterpart (886.12). Furthermore, the use of the log-spline distribution allows for a consistent method which can be applied readily across any watershed without careful calibration of the distribution function. Thus, the log-spline distribution was used for the regional growth curves. The lower values of the normalized discharge shown in Figure 7d for higher return periods (2-3) for the Ottawa River watershed suggest relatively more structural alternations within the watershed, for instance flood control and dams, than the Grand River watershed (Ottawa Riverkeeper, 2020). The Grand River watershed yielded relatively higher values of normalized discharge (>3) at higher return periods in Figure 7d. Figure 8 shows the comparison of estimated flood quantiles against theoretical flood quantiles at individual stations from both study watersheds for cases of high and low observation counts, such that "discharge count" refers to the number of years for which an annual maximum discharge was recorded (period of record). Return periods (T, years) have been converted in terms of the Gumbel reduced variable as follows:

$$Gumbel = -ln\left[ln\left(\frac{T}{T-1}\right)\right] \quad (10)$$

As expected, for the stations with high observation counts (n = 101 and n = 84 for the Grand River watershed (Figure 8a) and Ottawa River watershed (Figure 8b), respectively) the theoretical and estimated return periods are closer, at least for lower return periods. The value of long periods of record can also be considered in terms of the 5T threshold (shown as the dotted lines in Figure 8).

The 5T threshold requires that, for the reasonable estimation of a quantile for a desired return period T, there be at least 5T years of data (Hailegeorgis & Alfredsen, 2017).

The major limitations of this model stem from the nascent stage of the IDEAS geo-data model and the exclusion of hydrological processing algorithms. The initial offline GIS-processing entailed lengthy input data conversions to the IDEAS system prior to subsequent calculations. Furthermore, in contrast to the square raster where we have two orthogonal axis, the hexagonal cells in the IDEAS data model consists of a reference system of 3 non-orthogonal axis which makes the computation of the essential hydraulic parameters such as drainage direction and slope quite different from the traditional square raster system. Thus, GIS pre-processing computed on a square raster doesn't essentially hold true in case of IDEAS's hexagonal gridding system wherein subsequent calculations were performed, meriting additional development and testing.

3.2 Web-GIS Interface

A pre-alpha version of the InundatEd app is available at https://spatial.wlu.ca/inundated/. Source code for the most recent version of InundatEd will be publicly available on GitHub (Spatial Lab, 2020). The use of R/Shiny to develop InundatEd and its provision on GitHub encourages transparency, ongoing development, and response to user feedback and preferences.

3.3 Model Testing

The following return periods (in years) were observed for FEPs intersecting hydrometric station 02KF005 in the Ottawa River watershed: 26.5, 16.52, and 25.96. Additionally, a return period of 42.69 years was observed for a FEP intersecting hydrometric station 02KB001 in the Ottawa River watershed. The 100-year return period was tested for the Grand River watershed. Binary classification results for the Grand River watershed are shown in Figure 9 for four comparison metrics: Matthews Correlation Coefficient, Accuracy, True Positive Rate, and True Negative Rate. Figure 10 presents Matthews Correlation Coefficient and Accuracy results for the four Ottawa River watershed cases, with True Positive and True Negative results presented in Supplemetary Figure S4. Although the results for both the Grand River watershed and the Ottawa River watershed suggest substantial agreement between the respective observed and simulated flood extents, a number of considerations, including input data characteristics and metric bias, require

https://doi.org/10.5194/gmd-2020-316
Preprint. Discussion started: 28 October 2020

that the presented results be taken with caution and, in some cases, offer clear paths for improvement. With respect to input data, the simulated floods presented within this case study are limited by the initial use of a 30m x 30 DEM raster. As concluded by Papaioannou et al. (2016), floodplain modelling is sensitive to both the resolution of the input DEM and to the choice of modelling approach.

As noted in Lim & Brandt (2019), the reliability of the observed flood extent polygons also merits comment. In this case study, the observed FEPs for the Ottawa River watershed were originally digitized from remotely sensed data and thus carry forward the errors and uncertainties from prior processing. The Grand River watershed's 100-year return period extent was also generated outside of this study and potentially carries multiple sources of error and uncertainty. However, evaluation of the exact extent to which errors present in the observed flood extent polygons could have impacted the binary classification results was not an objective of this study.

With respect to the binary classification metrics for both watersheds, the generally high Accuracy values must also be taken with caution due to this metric's known overexaggeration of success in cases of unbalanced classes (Chicco & Jurman, 2020; Tharwat, 2018). This is particularly important to this case study since, for many reported subcatchments, the river channel accounts for much of the subcatchment's area, thus unbalancing the classification matrix in favour of positive observations. Thus, of the metrics reported herein, the Matthews Correlation Coefficient (MCC) is considered to be the most representative of the success of the simulated floods – it is robust against imbalanced classes while simultaneously requring high hit rates, low false alarms, high correct rejections, and low miss rates to yield a high value.

Figure 11 visualizes the 100-year return period simulated flood for the Grand River watershed. Although the colours of the simulated flood represents depth, the depth values have been excluded as the sole focus of this test is extent. Inset maps are provided which highlight one subcatchment with a high MCC (A, MCC= 0.95) and two subcatchments with low MCCs (B, MCC =0.34 and 0.38). The simulated flood shown in Figure 9A compares very well to the extent of its observed counterpart, suggesting that the high MCC values do represent areas of strong model success. Notably, three hydrometric stations are located within the Figure 11A subcatchment: 02GA014,

https://doi.org/10.5194/gmd-2020-316
Preprint. Discussion started: 28 October 2020

Geoscientific Model Development
Discussions

02GA027, and 02GA016. Per the methods in Section 2.2.2, station 02GA014 yielded a period of record of 54, 02GA027 yielded an insufficient (<10) period of record, and station 02GA016 yielded a period of record of 58. The presence of the two hydrometric stations with a considerable periods of record likely strengthened the regional regression of the area and contributed to the success of the simulated flood shown in Figure 11A. In contrast, within the low-MCC (0.34 and 0.38) subcatchments shown in Figure 11B the simulation considerably overestimated the extent of the 100-year return period flood. The overestimation of the flood extents observed in Figure 11B can likely be attributed, at least in part, to the following. It was observed (Figure S5) that dams (Grand River Conservation Authority, 2000) are located both upstream and downstream of the area shown in Figure 11B. The current iteration of the model makes no provision for flood mitigation structures. As such, the model has likely overestimated the discharge values at subcatchment outlets, particularly for those outlets which are a) relatively downstream in the watershed and b) impacted by nearby structures. However, it's possible to include such operations in future versions of the model by either modifying the DEM values to reflect flood control structures or by offsetting the discharge of the catchment based on structure storage.

With respect to the Ottawa River watershed, Figure 12 highlights subcatchments whose comparison between observed and simulated flood extents yielded low (A: MCC= 0.16 ; B: MCC= 0.29), moderate (D: MCC =0.67) and high (C: MCC = 0.91) MCC values. As with Figure 11, the colour of the simulated floods represnts depth, but depth values have been excluded as the sole focus of the MCC test is on flood extent. Figure 12A shows the simulated and observed flood extents for return period 25.69. Two main factors influencing the low MCC are readily apparent. The first is that the observed FEP appears "cut off", not extending through most of the subcatchment. It is possible that the flood in the remainder of the subcatchment was simply not digitized during the observed FEP's generation, especially given the subcatchment's position. However, of the area of the subcatchment intersected by the observed FEP, the simulated flood has considerably underestimated the observed flood extent. Figure 12B shows the extent comparison of the 42.69 -year return period in a subcatchment of low MCC (0.29). Interestingly, the simulated flood was not as vastly different from the observed flood as the very low MCC value might suggest, particulary with reference to Figure 11B, which yielded slightly higher (0.34 and 0.38) MCC values. The most visually prominent discrepancy in Figure 12B appears to be

https://doi.org/10.5194/gmd-2020-316
Preprint. Discussion started: 28 October 2020

connected to a false positive section near the south side of the subcatchment, which is consistent with the subcatchment's moderately high False Positive Rate (0.41) and high False Discovery Rate (0.84). Figure 12C illustrates a subcatchment of high MCC (0.91), characterized by an overall underestimation in flood extent, barring a slight overestimation in one area. Figure 12D (MCC = 0.67) shows a mixture of overestimation and underestimation.

Table 4 lists the number of subcatchments evaluated, the minimum MCC, the median MCC, and the maximum MCC for each of the 5 test return periods. The median MCC values ranged from 0.67 to 0.94, with both of those values coming from the Ottawa River watershed (return periods 42.69 and 26.5, respectively). The median MCC for the Grand River watershed was 0.84. Additionally, the median F_1 score (Chicco & Jurman, 2020) for the Grand River watershed was 0.85. The median F_1 scores for Ottawa River watershed return periods 26.5, 16.52, 25.96, and 42.69 were 0.96, 0.87, 0.90, and 0.65 respectively. Such results are approximately in line with Lim & Brandt (2019) which determined that low-resolution DEMs are capable of yielding relatively high comparison metrics (eg F_1 values approximateely >= 0.80) in situations where Manning's n varies widely over space. The connection between high values of Manning's n and flood overestimation (false discovery) was also discussed. The Grand River watershed yielded a median False Discovery Rate (FDR) of 0.20, and the four Ottawa River watershed cases yielded respective median FDRs of 0.019, 0.01, 0.006, and 0.44 for the evaluated subcatchments. The moderately high FDR value of 0.44 for the 42.69-year return period and the observed overestimation of flood extent (Figure 12B) may be a result of high local Manning's n values. In addition, the influences of flat terrain (Lim & Brandt, 2019) and anabranch must be considered as it can disrupt the assumption of a single drainiage direction for each pixel during subcatchment delineation. The topography of the area of the Ottawa River watershed wherein the extent comparisons were made is realtively flat with multiple anabranches and thus can lead to chaotic network delineation. Although attempts were made in this model to counter this impact and avoid slope values of 0 (the burning of the polyline network into the DEM, Section 2.2.1 and Figure 2), the use of the Manning's equation was still compromised in certain areas and likely had a negative impact on the resultant flood simulations.

https://doi.org/10.5194/gmd-2020-316
Preprint. Discussion started: 28 October 2020

Geoscientific Model Development Discussions

Overall, the results indicated that the current iteration of the InundatEd flood model was reasonably successful on the basis of moderate-high MCC values and direct comparisons. However, any weight assigned to this claim must, in addition to the previously discussed caveats, recall that only extent and not depth was compared between the observed and simulated floods. The use of the DGGS big-data architecture provides a promising foundation for further work, such as the incorporation of the impacts of flood control structures, on the InundatEd model.

3.4 Model Performance

Supplementary Figure S6 contrasts runtimes using the DGGS method against those using a traditional, raster-based method for sub-catchments within the Grand River Watershed (n= 306 for each method) during the generation of respective RP 100 flood maps. The mean runtime using the DGGS method (0.23 seconds) was significantly lower than the mean runtime using the raster-based method (3.98 seconds) at both the 99% confidence intervals ($p < 2.2e-16$). Thus, the efficiency of the proposed inundation model -coupled with a big-data Discrete Global Grids Systems architecture- is demonstrated with respect to processing times with limited input data. As the IDEAS framework and the InundatEd flood modelling method continue to develop, processing time benchmarks could be established to track and evaluate the model's robustness against increasing complexity (e.g., the integration of hydrological processing algorithms) and to facilitate comparisons with other inundation models.

3.5 Conclusions

We have tested a novel flood modelling and mapping system, implemented within a DGGS-based big data platform. In many parts of the world, including Canada, the widespread deployment of detailed hydrodynamic models has been hindered by complexities and expenses regarding input data and computational resources, especially the dichotomy between processing time and model complexity. This research proposes a novel solution to these challenges. First, we demonstrated the development of a flood modelling framework in a Discrete Global Grid Systems (DGGS) data model and the presentation of the models' outputs via an open-source R/Shiny interface robust against algorithm modifications and improvements. The DGGS data model efficiently integrates heterogeneous spatial data into a common framework, rapidly develops models, and can scale for thousands of unit processing regions through easy parallelization. Second, the use of the

https://doi.org/10.5194/gmd-2020-316
Preprint. Discussion started: 28 October 2020

catchment-integrated Manning's equation avoids high-uncertainty river cross-sections and produces physically justified flood inundation extents. Third, DGGS-powered analytics allow users to quickly visualize flood extents and depths for regions of interest, with reasonable alignment with observed flooding events. Finally, we believe our flood-inundation estimation method can address situations where good quality data is scarce and/or there are insufficient resources for a complex model. To apply the model in a real time environment we would need a discharge forecasting model or have real-time discharge data at the catchment outlet, which could be used to compute the flood inundation using the pre-computed stage-discharge relationship and inundation model.

https://doi.org/10.5194/gmd-2020-316
Preprint. Discussion started: 28 October 2020

4. References

Albano, R., Sole, A., Adamowski, J., Perrone, A., & Inam, A. (2018). Using FloodRisk GIS freeware for uncertainty analysis of direct economic flood damages in Italy. *International Journal of Applied Earth Observation and Geoinformation*, *73*, 220–229. https://doi.org/10.1016/j.jag.2018.06.019

Appelhans, T., & Fay, C. (2019). leafgl: Bindings for Leaflet.glify. R package version 0.1.1.

Attari, M., & Hosseini, S. M. (2019). A simple innovative method for calibration of Manning's roughness coefficient in rivers using a similarity concept. *Journal of Hydrology*, *575*, 810–823. https://doi.org/10.1016/j.jhydrol.2019.05.083

Brunner, G. W. (2016). *HEC-RAS River Analysis System 2D Modelling User's Manual Version 5.0.* (Report Number CPD-68A). US Army Corps of Engineers Hydrologic Engineering Center.

Burrell, B., & Keefe, J. (1989). Flood risk mapping in new brunswick: A decade review. *Canadian Water Resources Journal*, *14*(1), 66–77. https://doi.org/10.4296/cwrj1401066

Calamai, L., & Minano, A. (2017). Emerging trends and future pathways: A commentary on the present state and future of residential flood insurance in Canada. *Canadian Water Resources Journal*, *42*(4), 307–314. https://doi.org/10.1080/07011784.2017.1362358

Canada Centre for Mapping and Earth Observation (2015). *Canadian Digital Elevation Model, 1945-2011 (Record ID 7f245e4d-76c2-4caa-951a-45d1d2051333).* [Data set]. Natural Resources Canada. Retrieved from https://open.canada.ca/data/en/dataset/7f245e4d-76c2-4caa-951a-45d1d2051333#wb-auto-6

Canada Centre for Remote Sensing (2019). *2015 Land Cover of Canada (Record ID 4e615eae-b90c-420b-adee-2ca35896caf6)*. [Data set]. Natural Resources Canada. Retrieved from https://open.canada.ca/data/en/dataset/4e615eae-b90c-420b-adee-2ca35896caf6

Centre For Research On The Epidemiology Of Disasters – CRED (2015). *"The human cost of natural disasters" – 2015: A global perspective*. CRED: Brussels. Accessed from https://www.cred.be/index.php?q=HCWRD.

Chicco, D., & Jurman, G. (2020). The advantages of the Matthews correlation coefficient (MCC) over F1 score and accuracy in binary classification evaluation. *BMC Genomics, 21,*6. doi: 10.1186/s12864-019-6413-7.

Chow, V.T. (1959). *Open-channel hydraulics. McGraw-Hill.*

Comber, A., & Wulder, M. (2019). Considering spatiotemporal processes in big data analysis: Insights from remote sensing of land cover and land use. *Transactions in GIS, 23(5)*, 879–891. https://doi.org/10.1111/tgis.12559

Craglia, M., de Bie, K., Jackson, D., Pesaresi, M., Remetey-Fülöpp, C., Wang, C., et al. (2012). Digital Earth 2020: Towards the vision for the next decade. *Int. J. Digital Earth, 5(1)*,4-21. 10.1080/17538947.2011.638500

Craglia, M., Goodchild, M.F., Annoni, A., Câmara, G., Gould, M.D., Kuhn, W., et al. (2008). Next-Generation Digital Earth (Editorial). *Int. J. Spat. Data Infrastruct. Res., 3*,146-167. 10.2902/1725-0463.2008.03.art9.

Darlymple, T. (1960). *Rep. No Water Supply Paper 1543-A.* U.S. Geological Survey, Reston, VA, U .S.

Eaton, B., Church, M., & Ham, D. (2002). Scaling and regionalization of flood flows in British Columbia, Canada. *Hydrol. Processes 16*, 3245–3263, http://dx.doi.org/10.1002/hyp.1100.

https://doi.org/10.5194/gmd-2020-316
Preprint. Discussion started: 28 October 2020

Environment and Climate Change Canada (2019). *An Examination of Governance, Existing Data, Potential Indicators and Values in the Ottawa River Watershed. I*SBN: 978-0-660-31053-4

Ferrari, A., Dazzi, S., Vacondio, R., & Mignosa, P. (2020). Enhancing the resilience to flooding induced by levee breaches in lowland areas: a methodology based on numerical modelling. *Nat. Hazards Earth Syst. Sci., 20*, 59–72.

Fouad, G., Skupin, A., & Tague, C. L. (2016). Regional regression models of percentile flows for the contiguous US: Expert versus data-driven independent variable selection. *Hydrology and Earth Systems Sciences Discussions, 17*, 1-33. 10.5194/hess-2016-639.

Garousi-Nejad, I., Tarboton, D.G., Aboutalebi, M., & Torres-Rua, A. F. (2019). Terrain analysis enhancements to the Height Above Nearest Drainage flood inundation mapping method. *Water Resources Research, 55*, 7983-8009. https://doi.org/10.1029/2019WR024837

Gebetsroither-Geringer, E., Stollnberger, R., & Peters-Anders, J. (2018). Interactive Spatial Web-Applications as New Means of Support for Urban Decision-Making Processes. In *ISPRS Annals of the Photogrammetry, Remote Sensing and Spatial Information Sciences* (Vol. 4, pp. 59–66). Delft, The Netherlands. https://doi.org/10.5194/isprs-annals-IV-4-W7-59-2018

Goteti, Gopi (2014). hazus: Damage functions from FEMA's HAZUS software for use in modeling financial losses from natural disasters. R package version 0.1. Retrieved from https://CRAN.R-project.org/package=hazus

Grand River Conservation Authority (2019). *Regulatory Floodplain* [Data set]. Grand River Conservation Authority. https://data.grandriver.ca/downloads-geospatial.html

Grand River Conservation Authority (2014). *Grand River Watershed Water Management Plan Executive Summary - March 2014*. Cambridge, ON. Retrieved from https://www.grandriver.ca.

Grand River Conservation Authority (2000). *Dams*. [Data set]. Grand River Conservation Authority. https://data.grandriver.ca/downloads-geospatial.html.

Haddad, K., Rahman, A., & Kuczera, G. (2011). Comparison of Ordinary and Generalised Least Squares Regression Models in Regional Flood Frequency Analysis: A Case Study for New South Wales. *Australasian Journal of Water Resources, 15(1),* 59-70, doi: 10.1080/13241583.2011.11465390

Handmer, J. W. (1980). Flood hazard maps as public information: An assessment within the context of the Canadian flood damage reduction program. *Canadian Water Resources Journal*, *5*(4), 82–110. https://doi.org/10.4296/cwrj0504082

Hailegeorgis, T. T., & Alfredsen, K. (2017). Regional flood frequency analysis and prediction in ungauged basins including estimation of major uncertainties for mid-Norway. *Journal of Hydrology: Regional Studies, 9*, 104-126.

Hutchinson, David. (2016). HYDAT: An interface to Canadian Hydrometric Data. R package version 1.0. [GitHub Repository]. Retrieved from https://github.com/CentreForHydrology/HYDAT.git

Kalyanapu, A. J., Shankar, S., Pardyjak, E. R., Judi, D. R., & Burian, S. J. (2011). Assessment of GPU computational enhancement to a 2D flood model. *Environmental Modelling and Software*, *26*(8), 1009–1016. https://doi.org/10.1016/j.envsoft.2011.02.014

Kamal, V., Mukherjee, S., Singh, P. *et al.* (2017). Flood frequency analysis of Ganga river at Haridwar and Garhmukteshwar. *Appl Water Sci* **7,** 1979–1986. https://doi.org/10.1007/s13201-016-0378-3

https://doi.org/10.5194/gmd-2020-316
Preprint. Discussion started: 28 October 2020

Geoscientific Model Development Discussions

Kaur, B., Shrestha, N. K., Daggupati, P., Rudra, R. P., Goel, P. K., Shukla, R., Allataifeh, N. (2019). Water Security Assessment of the Grand River Watershed in Southwestern Ontario, Canada. *Sustainability, 11(7).* doi: http://dx.doi.org/10.3390/su11071883.

Langat, P.K., Kumar, L., & Koech, R. (2019). Identification of the Most Suitable Probability Distribution Models for Maximum, Minimum, and Mean Streamflow. *Water*, *11*, 734.

Lim, N. J., & Brandt, S. A. (2019). Are Feature Agreement Statistics Alone Sufficient to Validate Modelled Flood Extent Quality? A Study on Three Swedish Rivers Using Different Digital Elevation Model Resolutions. *Mathematical Problems in Engineering, 2019,* 9816098. https://doi.org/10.1155/2019/9816098.

Li, Z., Huang, G., Wang, X., Han, J., Fan, Y. (2016). Impacts of future climate change on river discharge based on hydrological interference: a case study of the Grand River Watershed in Ontario, Canada. *Science of the Total Environment*, *548-549, 198-210.* https://doi.org/10.1016/j.scitotenv.2016.01.002.

Nastev, M., & Todorov, N. (2013). Hazus: A standardized methodology for flood risk assessment in Canada. *Canadian Water Resources Journal*, *38*(3), 223–231. https://doi.org/10.1080/07011784.2013.801599.

Natural Resources Canada (2018). *Floods in Canada -Archive (Record ID 74144824-206e-4cea-9fb9-72925a128189).* [Data set]. Natural Resources Canada. Retrieved from https://open.canada.ca/data/en/dataset/74144824-206e-4cea-9fb9-72925a128189.

Natural Resources Canada (2020). *Flood in Canada Product Specifications.*

Neal, J., Dunne, T., Sampson, C., Smith, A., & Bates, P. (2018). Optimisation of the two-dimensional hydraulic model LISFOOD-FP for CPU architecture. *Environmental Modelling and Software*, *107*(May), 148–157. https://doi.org/10.1016/j.envsoft.2018.05.011

Nix, G. A. (1987). Management of the Ottawa River Basin. *Water International, 12(4),* 183-188.

Nobre, A. D., Cuartas, L. A., Momo, M. R., Severo, D. L., Pinheiro, A., & Nobre, C. A. (2016). HAND contour: A new proxy predictor of inundation extent. *Hydrological Processes 30(2)*: 320-333. doi: 10.1002/hyp.10581

Ottawa Riverkeeper. (2020). *Dams*. [Website] Accessed at https://www.ottawariverkeeper.ca/home/explore-the-river/dams/.

Oubennaceur, K., Chokmani, K., Nastev, M., Lhissou, R., & El Alem, A. (2019). Flood risk mapping for direct damage to residential buildings in Quebec, Canada. *International Journal of Disaster Risk Reduction*, *33*, 44–54. https://doi.org/10.1016/j.ijdrr.2018.09.007

Pal, K. (2002). Assessing Community Vulnerability to Flood Hazard in Southern Ontario. *Canadian Water Resources Journal, 27 (2),* 155-173.

Papaioannou, G., Loukas, A., Vasiliades, L., & Aronica, G. T. (2016). Flood inundation mapping sensitivity to riverine spatial resolution and modelling approach. *Nat Hazards, 83,* S117-S132. 10.1007/s11069-016-2382-1.

Rahmati, O., Kornejady, A., Samadi, M., Nobre, A. D., & Melesse, A. M. (2018). Development of an automated GIS tool for reproducing the HAND terrain model. *Environmental Modelling and Software*, *102*, 1–12. https://doi.org/10.1016/j.envsoft.2018.01.004

R Core Team (2019). R: A language and environment for statistical computing. R Foundation for Statistical Computing, Vienna, Austria. https://www.R-project.org/.

Rennó, C.D., Nobre, A.D., Cuartas, L.A., Soares, J.V., Hodnett, M.G., Tomasella, J., & Waterloo, M. (2008). HAND, a new terrain descriptor using SRTM-DEM; mapping terra-firme rainforest environments in Amazonia. *Remote Sensing of Environment 112*, 3469–3481.

https://doi.org/10.5194/gmd-2020-316
Preprint. Discussion started: 28 October 2020

Geoscientific Model Development Discussions
Open Access EGU

Robert, B., Forget, S., & Rousselle, J. (2003). The Effectiveness of Flood Damage Reduction Measures in the Montreal Region. *Natural Hazards*, *28*, 367–385. Retrieved from https://journals.scholarsportal.info/pdf/0921030x/v28i2-3/367_teofdrmitmr.xml

Robertson, C., Chaudhuri, C., Hojati, M., & Roberts, S. (2020). An integrated environmental analytics system (IDEAS) based on a DGGS. *ISPRS Journal of Photogrammetry and Remote Sensing*, *162*, 214-228.

Robson, A. J., & Reed, D. W. (1999). *Flood Estimation Handbook, vol. 3 Statistical Procedures for Flood Frequency Estimation.* Institute of Hydrology, Wallingford, UK.

Rodda, Harvey J. (2005). The development and application of a flood risk model for the Czech Republic. *Natural hazards 36(1-2)*: 207-220. doi: 10.1007/s11069-004-4549-4

Salas, J. D., & Obeysekera J. (2014). Revisiting the Concepts of Return Period and Risk for Nonstationary Hydrologic Extreme Events, *J. Hydrol. Eng*,*19*, 554-568.

Samela, C., Albano, R., Sole, A., & Manfreda, S. (2018). A GIS tool for cost-effective delineation of flood-prone areas. *Computers, Environment, and Urban Systems, 70,* 43-52. https://doi.org/10.1016/j.compenvurbsys.2018.01.013

Samela, C., Troy, T. J., & Manfreda, S. (2017). Geomorphic classifiers for flood-prone areas delineation for data-scarce environments. *Advances in Water Resources*, *102,* 13-28. http://dx.doi.org/10.1016/j.advwatres.2017.01.007

Singh, Vijay P.(2015). *Entropy Theory in Hydrologic Science and Engineering*. McGraw-Hill Education: New York, Chicago, San Francisco, Athens, London, Madrid, Mexico City, Milan, New Delhi, Singapore, Sydney, Toronto. Accessed at: https://www.accessengineeringlibrary.com/content/book/9780071835466

Song, S., Schmalz, B., Zhang, J. X., Li, G., & Fohrer, N. (2017). Application of modified Manning formula in the determination of vertical profile velocity in natural rivers. *Hydrology Research, 48(1),* 133–146. doi: https://doi.org/10.2166/nh.2016.131

Spatial Lab (2020). InundatEd. [Github Repository]. Retrieved from https://github.com/thespatiallabatLaurier/floodapp_public

Stephens, E., & Bates, P. (2015). Assessing the reliability of probabilistic flood inundation model predictions. *Hydrol. Process. 29*, 4264–4283. doi: 10.1002/hyp.10451.

Stevens, M. R., & Hanschka, S. (2014). Municipal flood hazard mapping: the case of British Columbia, Canada. *Natural Hazards*, *73*, 907–932. https://doi.org/10.1007/s11069-014-1117-4

Stone, C. J., Hansen, M. H., Kooperberg, C., & Truong, Y. K. (1997). Polynomial Splines and their Tensor Products in Extended Linear Modeling. *The Annals of Statistics*, *25*(4), 1371–1425.

Strategic Policy and Innovation Centre (2019). *Lakes, Rivers and Glaciers in Canada – CanVec Series – Hydrographic Features (Record ID 9d96e8c9-22fe-4ad2-b5e8-94a6991b744b).* [Data set]. Natural Resources Canada. https://open.canada.ca/data/en/dataset/9d96e8c9-22fe-4ad2-b5e8-94a6991b744b

Tarboton, D. G. (2005). Terrain Analysis Using Digital Elevation Models Version 5 [Computer Software]. Utah State University, Logan. Retrieved from http://hydrology.usu.edu/taudem/taudem5/downloads.html

Tarboton, D. G., & Ames, D. P. (2004). Advances in the mapping of flow networks from digital elevation data. *Bridging the Gap: Meeting the World's Water and Environmental Resources Challenges - Proceedings of the World Water and Environmental Resources Congress*

https://doi.org/10.5194/gmd-2020-316
Preprint. Discussion started: 28 October 2020

2001, *111*(435), 1–10. https://doi.org/10.1061/40569(2001)166

Tavares da Costa, R., Manfreda, S., Luzzi, V., Samela, C., Mazzoli, P., Castellarin, A., & Bagli, S. (2019). A web application for hydrogeomorphic flood hazard mapping. *Environmental Modelling & Software*, *118*, 172-186. https://doi.org/10.1016/j.envsoft.2019.04.010.

Teng, J., Jakeman, A. J., Vaze, J., Croke, B. F. W., Dutta, D., & Kim, S. (2017). Flood inundation modelling: A review of methods, recent advances and uncertainty analysis. *Environmental Modelling and Software*, *90*, 201–216. https://doi.org/10.1016/j.envsoft.2017.01.006

Teng, J., Vaze, J., Kim, S., Dutta, D., Jakeman, A. J., & Croke, B. F. W. (2019). Enhancing the Capability of a Simple, Computationally Efficient, Conceptual Flood Inundation Model in Hydrologically Complex Terrain. *Water Resources Management*, *33*(2), 831–845. https://doi.org/10.1007/s11269-018-2146-7

Tharwat, A. (2018). Classification assesment methods. *Applied Computing and Informatics. https://doi.org/10.1016/j.aci.2018.08.003.*

Thistlethwaite, J., Henstra, D., Brown, C., & Scott, D. (2018). How Flood Experience and Risk Perception Influences Protective Actions and Behaviours among Canadian Homeowners. *Environmental Management*, *61*(2), 197–208. https://doi.org/10.1007/s00267-017-0969-2

Thistlethwaite, J., Henstra, D., Peddle, S., & Scott, D. (2017). *Canadian Voices on Changing Flood Risk: Findings from a National Survey*. Waterloo. Retrieved from https://uwaterloo.ca/climate-centre/sites/ca.climate-centre/files/uploads/files/canadian_voices_on_changing_flood_risk_fnl.pdf

Towe, R., Dean, G., Edwards, L., Nundloll, V., Blair, G., Lamb, R., Hankin, B., & Manson, S. (2020). Rethinking data-driven decision support in flood risk management for a big data age. *J Flood Risk Management, e12652*. https://doi.org/10.1111/jfr3.12652.

Tullis, B. P. (2012). *NCHRP Report 734 Hydraulic Loss Coefficients for Culverts.* Transportation Research Board, Washington, D. C. Accessed at: https://www.nap.edu/read/22673/chapter/1.

Vacondio, R., Palù, A., Ferrari, A., Mignosa, P., Aureli, F., & Dazzi, S. (2017). A non-uniform efficient grid type for GPU-parallel Shallow Water Equations models. *Environmental Modelling & Software 88*, 119-137

Veale, B., & Cooke, S. (2017). Implementing integrated watershed management: illustrations from the Grand River watershed. *International Journal of Water Resources Development*, *33(3)*, 375-392

Vojtek, M., & Vojteková, J. (2016). Flood hazard and flood risk assessment at the local spatial scale: a case study. *Geomatics, Natural Hazards and Risk*, *7*(6), 1973–1992. https://doi.org/10.1080/19475705.2016.1166874

Wang, L., & Cheng, Q. (2007). Design and implementation of a web-based spatial decision support system for flood forecasting and flood risk mapping. *International Geoscience and Remote Sensing Symposium (IGARSS)*, 4588- 4591. https://doi.org/10.1109/IGARSS.2007.4423879

Wang, Y., & Yang, X. (2020). A Coupled Hydrologic–Hydraulic Model (XAJ–HiPIMS) for Flood Simulation. *Water, 12,* 1288. https://doi.org/10.3390/w12051288.

Werstuck, C., Coulibaly, P. (2017). Hydrometric network design using dual entropy multi-objective optimization in the Ottawa River Basin. *Hydrology Research, 48(6),* 1639-1651.

Wilby, R. L., & Keenan, R. (2012). Adapting to flood risk under climate change. *Progress in Physical Geography*, *36*(3), 348–378.

https://doi.org/10.5194/gmd-2020-316
Preprint. Discussion started: 28 October 2020

Wilson, D., Fleig, A. K., Lawrence, D., Hisdal, H., Pettersson, L. E., & Holmqvist. E. (2011). *A review of NVE's flood frequency estimation procedures.* Norwegian Water Resources and Energy Directorate Report no. 9.

Wing, O. E. J., Bates, P. D., Sampson, C. C., Smith, A. M., Johnson, K. A., & Erickson, T. A. (2017). Validation of a 30 m resolution flood hazard model of the conterminous United States. *Water Resour. Res.*, *53*,7968–7986, doi:10.1002/2017WR020917.

Xing, Y., Liang, Q., Wang, G., Ming, X., & Xia, X. (2019). City-scale hydrodynamic modelling of urban flash floods: the issues of scale and resolution. *Natural Hazards, 96,* 473 - 496. https://doi.org/10.1007/s11069-018-3553-z

https://doi.org/10.5194/gmd-2020-316
Preprint. Discussion started: 28 October 2020

Geoscientific Model Development Discussions
Open Access

List of tables:

Table 1. Values of Manning's n

NRCAN LULC Value	NRCAN Description	Manning's n
1	Temperate or sub-polar needleleaf forest	0.16
2	Sub-polar taiga needleleaf forest	0.16
5	Temperate or sub-polar broadleaf deciduous forest	0.16
6	Mixed forest	0.16
8	Temperate or sub-polar shrubland	0.1
10	Temperate or sub-polar grassland	0.035
12	Sub-polar or polar grassland-lichen-moss	0.035
13	Sub-polar or polar barren-lichen-moss	0.03
14	Wetland	0.1
15	Cropland	0.035
16	Barren lands	0.025
17	Urban	0.08
18	Water	0.04

https://doi.org/10.5194/gmd-2020-316
Preprint. Discussion started: 28 October 2020

Geoscientific Model Development Discussions

Table 2. Study Watershed Characteristics

Characteristic	**Grand River Watershed**	**Ottawa River Watershed**
Drainage Area (km^2)	6,800 (Li et al., 2016)	146,000 (Nix, 1987)
Elevation range (masl)	173-535 (Lake Erie Source Protection Region Technical Team, 2008)	430 – 20 (Nix, 1987)
Geologic characteristics	Underlain by groundwater-rich, fractured, porous limestone bedrock; surface geology characterized by glacial till and moraine complexes (Liel et al., 2016)	Incorporates the geological subdivisions St. Lawrence Lowlands, Grenville Province, Superior Province, and Cobalt Plate within the region of the Canadian Shield (Environment and Climate Change Canada, 2019)
Approximate Population size	985,000 (Grand River Conservation Authority, 2014)	> 2,000,000 (Environment and Climate Change Canada, 2019)
Land Use / Land Cover	43% agriculture; 26.92% range-grass and pasture; 12% forests; 9.29 % urban areas; 1.8% wetlands (Veale & Cooke, 2017)	73% forested (Quebec); 85% mixed and deciduous forest, 15% boreal (middle-south and northern regions, respectively) (Environment and Climate Change Canada, 2019); 6% farmland; <2% developed (Werstuck & Coulibaly, 2017)
Average Annual Precipitation (mm)	800-900 (Kaur et al., 2019)	840 (Werstuck & Coulibaly, 2017)
Temperature	8-10 ° C average annual; moderate-to-cool temperate (Kaur et al., 2019)	21 - -10 °C average daily (Werstuck & Coulibaly, 2017)

https://doi.org/10.5194/gmd-2020-316
Preprint. Discussion started: 28 October 2020

Geoscientific Model Development Discussions
Open Access
EGU

Table 3. Simulated Flood Generation – Ottawa River Watershed

Observed Flood Extent Polygon	**Observed Date and Time (UTC)**	**Intersected Hydrometric Station**	**Station Period of Record (years)**	**Index Flood ($\tilde{Q}$, m^3s^{-1})**	**Observed Discharge (m^3s^{-1})**	**Logspline fit observation count**	**Cumulative Probability Value**	**Return Period (years)**
FloodExtentPolygon_QC_LowerOttawa_20190429_230713.shp	2019/04/29 23:07:13	02KF005	38	3400	5790	1487	0.962	26.5
FloodExtentPolygon_QC_LowerOttawa_20190507_111329.shp	2019/05/07 11:13:29	02KF005	38	3400	5350	1487	0.939	16.52
FloodExtentPolygon_QC_LowerOttawa_20190513_225800.shp	2019/05/13 22:58:00	02KF005	38	3400	5570	1487	0.961	25.96
FloodExtentPolygon_QC_CentralOttawa_20190503_113004.shp	2019/05/03 11:30:04	02KB001	52	258	477	1487	0.977	42.69

https://doi.org/10.5194/gmd-2020-316
Preprint. Discussion started: 28 October 2020

Geoscientific Model Development
Discussions
Open Access

Table 4. Matthews Correlation Coefficient Results

Watershed	**Return Period (years)**	**Number of evaluated subcatchments**	**Minimum MCC**	**Median MCC**	**Maximum MCC**
Grand River	100	71	0.33	0.84	0.98
Ottawa River	26.5	17	0.49	0.94	1.00
Ottawa River	16.52	21	0.13	0.80	1.00
Ottawa River	25.96	22	0.16	0.85	1.00
Ottawa River	42.69	7	0.29	0.67	0.74

https://doi.org/10.5194/gmd-2020-316
Preprint. Discussion started: 28 October 2020

Geoscientific Model Development
Discussions
Open Access
EGU

List of Figures

Figure 1. GIS Input Data – Grand River Watershed (a) and Ottawa River Watershed (b) Topography. The maps are created in Qgis with the basemaps provided by © Google Satellite Maps under OpenLayerPlugin.

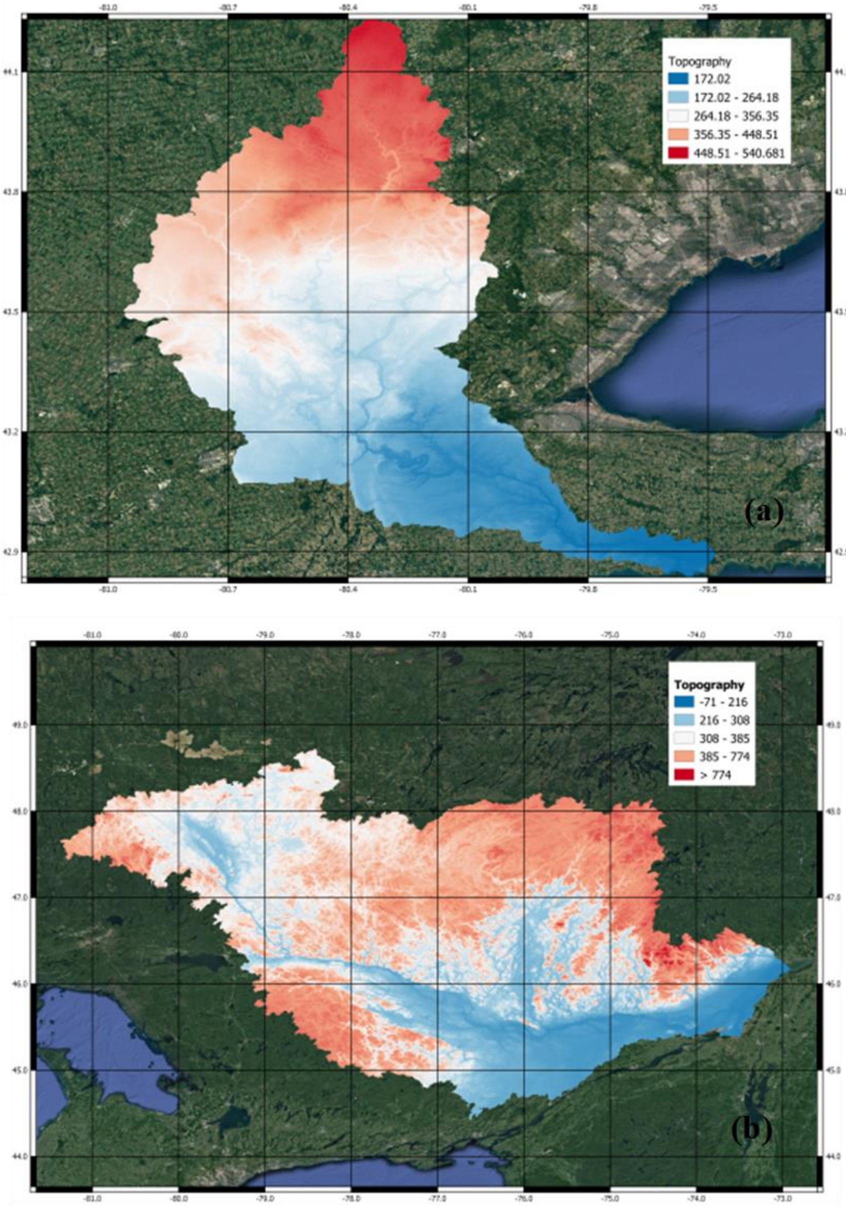

https://doi.org/10.5194/gmd-2020-316
Preprint. Discussion started: 28 October 2020

Figure 2. Flood Modelling Stage 1: GIS Preprocessing

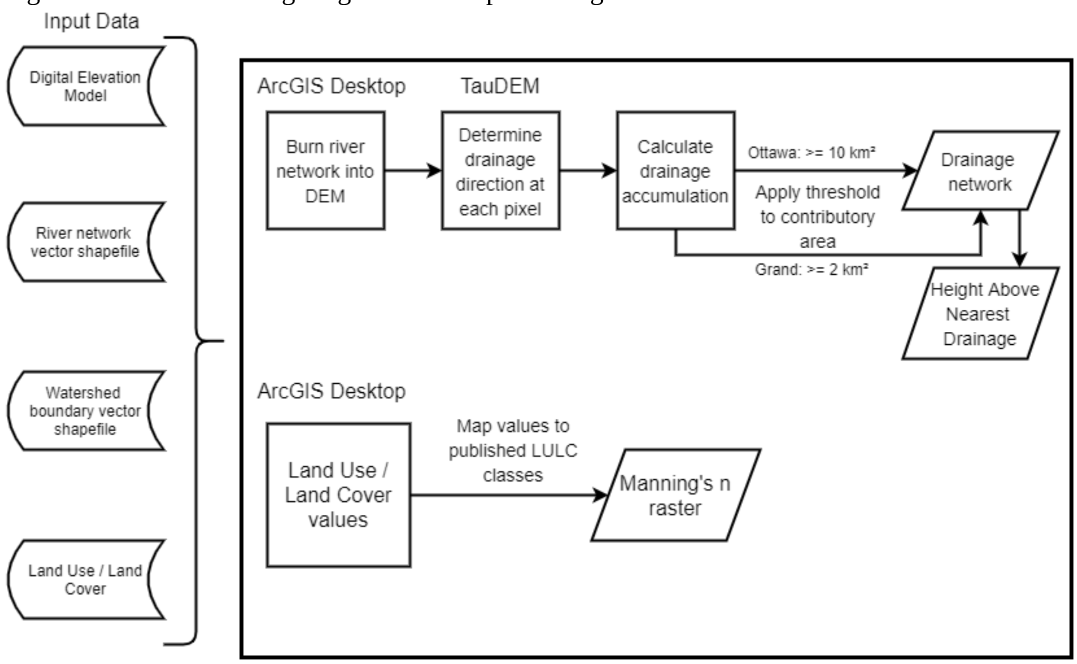

https://doi.org/10.5194/gmd-2020-316
Preprint. Discussion started: 28 October 2020

Figure 3. Flood Modelling Stage 2: Flood Frequency Analysis and Regional Regression

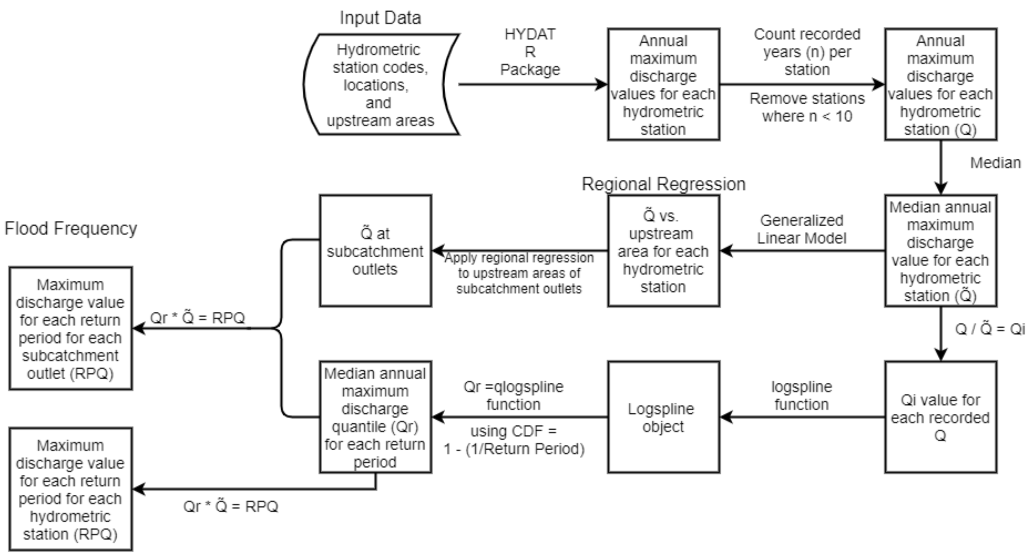

Figure 4. Flood Modelling Stage 3: Catchment Integrated Manning's Equation

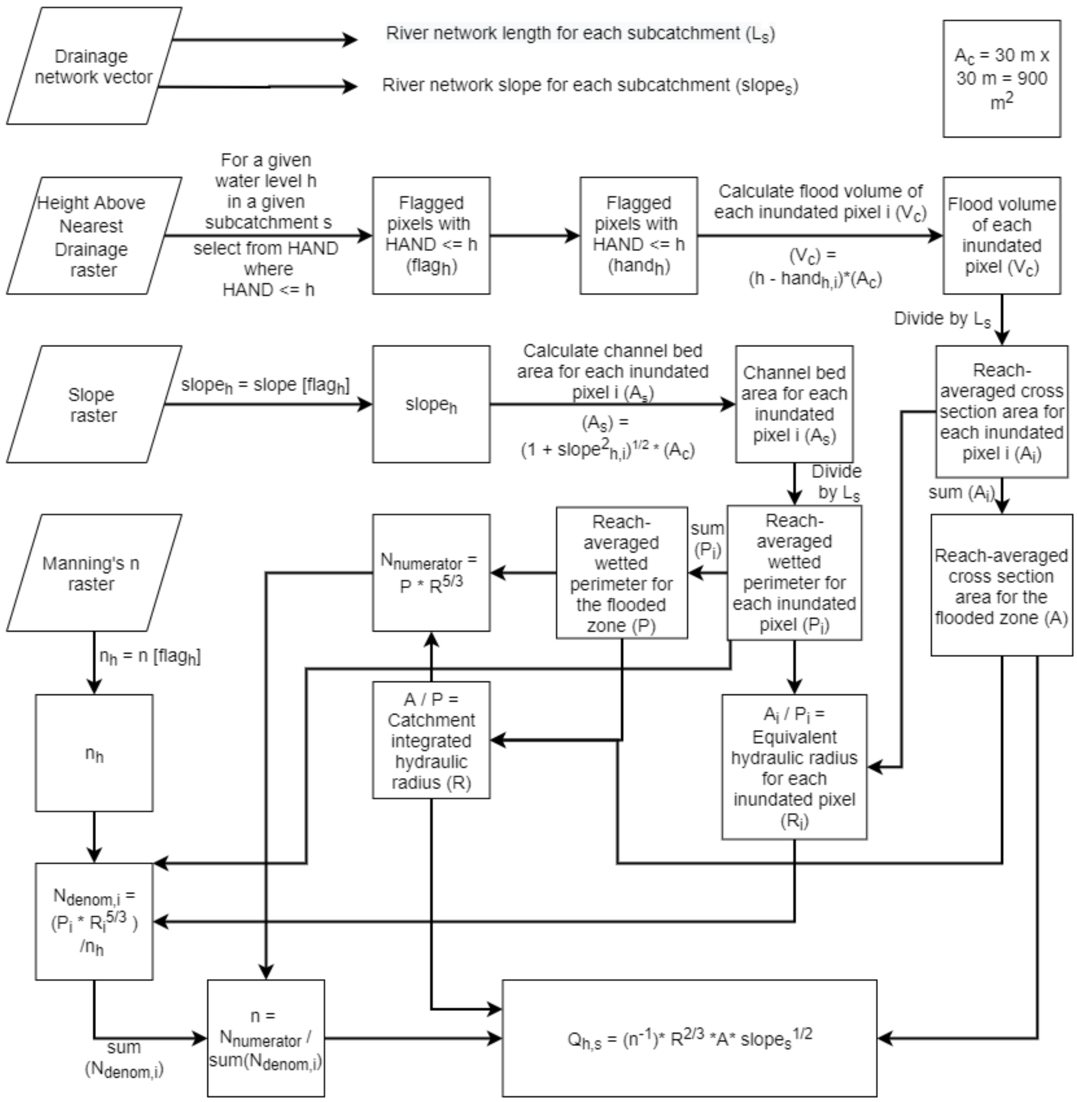

https://doi.org/10.5194/gmd-2020-316
Preprint. Discussion started: 28 October 2020

Geoscientific Model Development Discussions

Figure 5. InundatEd User Interface (a) and System Diagram (b). The basemap is created in Leaflet using © OpenStreetMap contributors 2020. Distributed under a Creative Commons BY-SA License

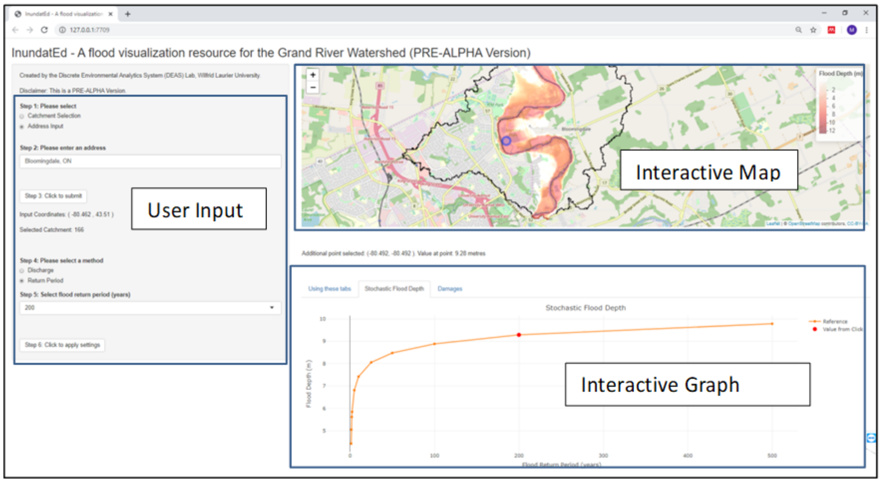

a) InundatEd User Interface

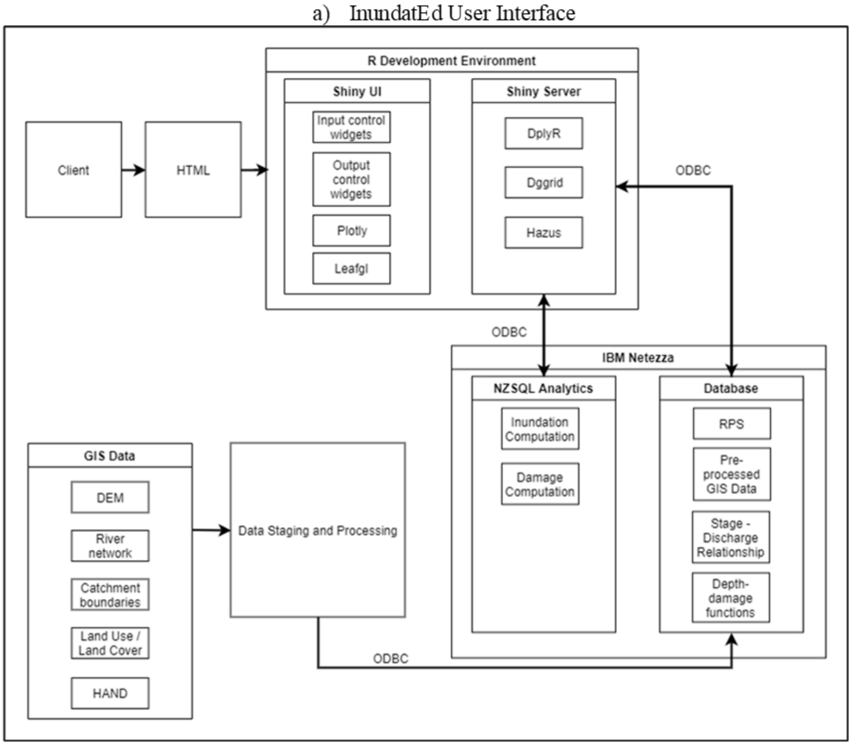

b) InundatEd System Diagram

https://doi.org/10.5194/gmd-2020-316
Preprint. Discussion started: 28 October 2020

Geoscientific Model Development
Discussions

Figure 6. GIS processing outputs for the Grand River Watershed and the Ottawa River Watershed: Height Above Nearest Drainage (a-b), Drainage network (c-d), and Manning's n values (e-f). The maps are created in Qgis with the basemaps provided by © Google Satellite Maps and © Google Street Maps under OpenLayerPlugin.

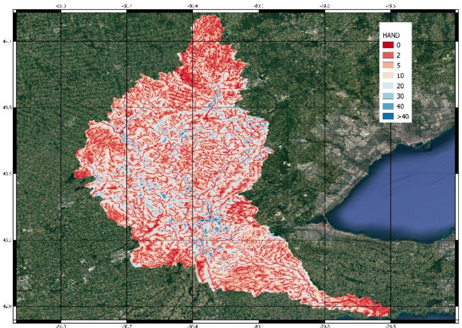

a) Grand River Watershed Height Above Nearest Drainage

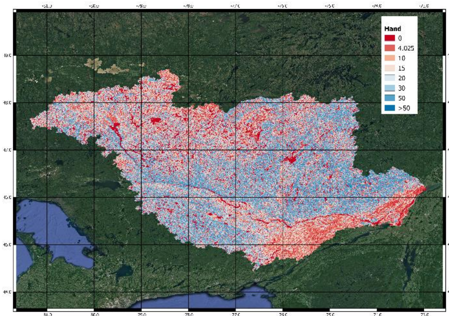

b) Ottawa River Watershed Height Above Nearest Drainage

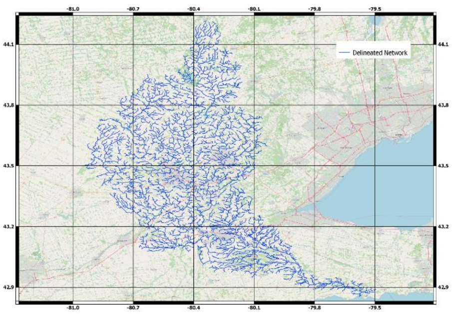

c) Grand River Watershed Drainage Network

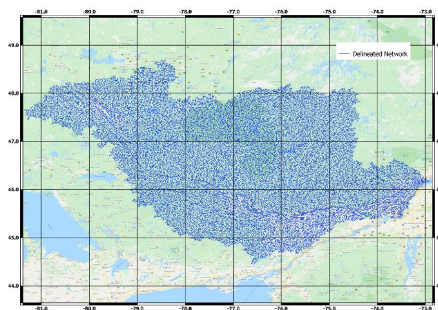

d) Ottawa River Watershed Drainage Network

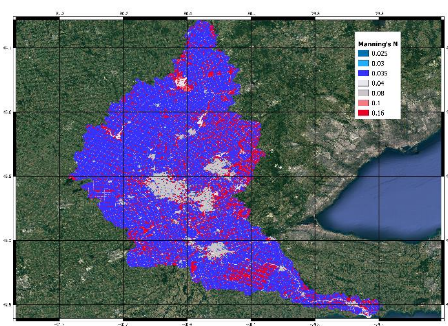

e) Grand River Watershed Manning's n

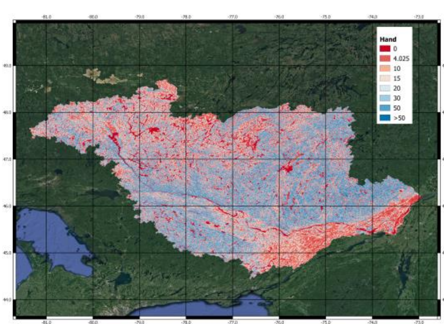

f) Ottawa River Watershed Manning's n

https://doi.org/10.5194/gmd-2020-316
Preprint. Discussion started: 28 October 2020

Geoscientific Model Development
Discussions
Open Access
EGU

Figure 7. Flood frequency and regional regression plots

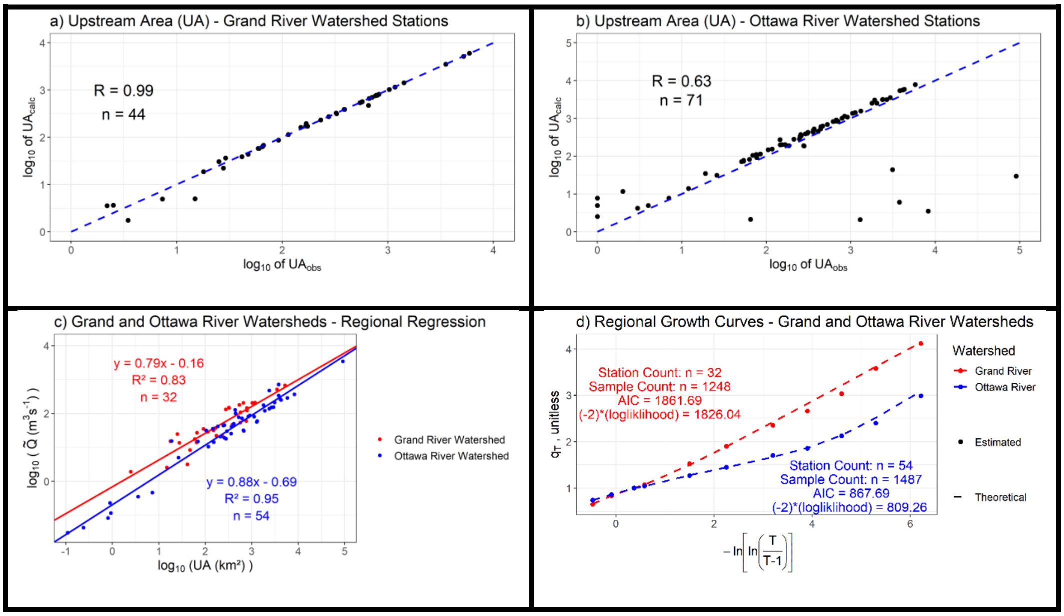

Geoscientific Model Development Discussions
Open Access
EGU

Figure 8. Theoretical Versus Estimated Flood Quantiles

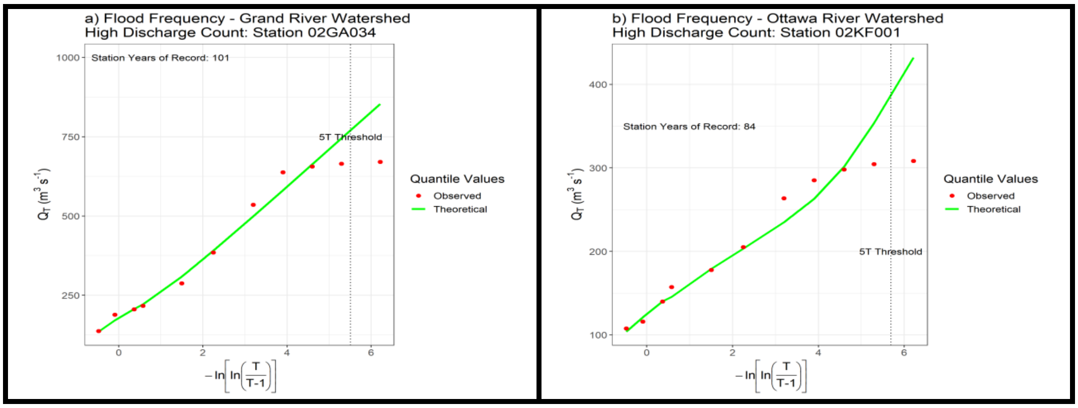

Geoscientific Model Development
Open Access
Discussions

Figure 9. Binary Classification Results – Grand River Watershed

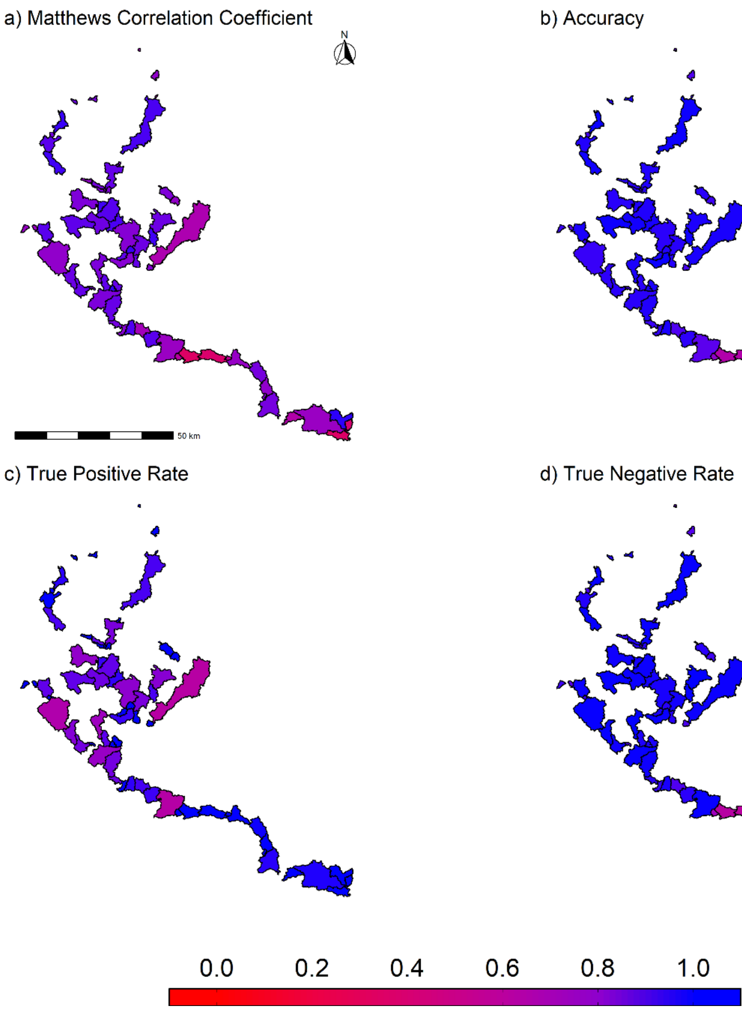

https://doi.org/10.5194/gmd-2020-316
Preprint. Discussion started: 28 October 2020

Geoscientific Model Development Discussions

Figure 10. Binary Classification Results – Ottawa River Watershed

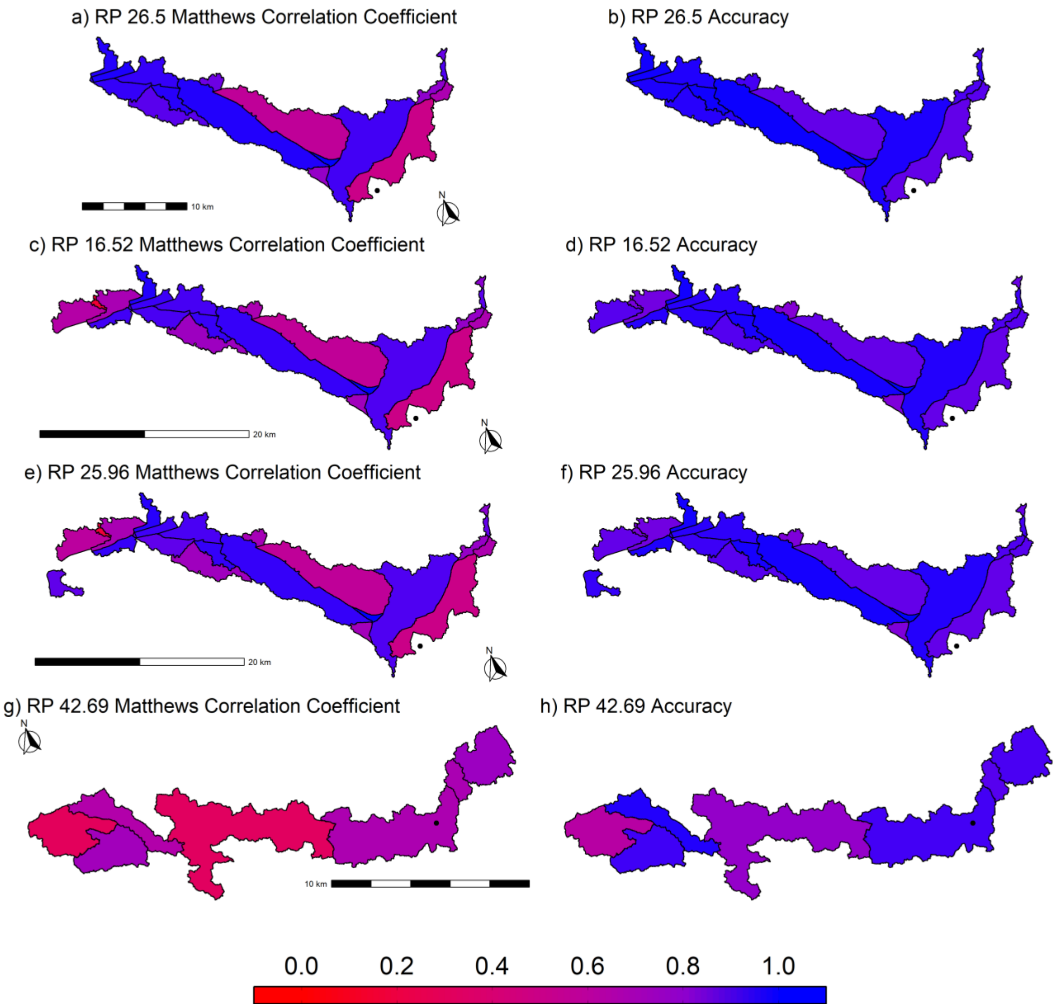

https://doi.org/10.5194/gmd-2020-316
Preprint. Discussion started: 28 October 2020

Figure 11. Simulated Flood and Insets – Grand River Watershed 100-Year Return Period

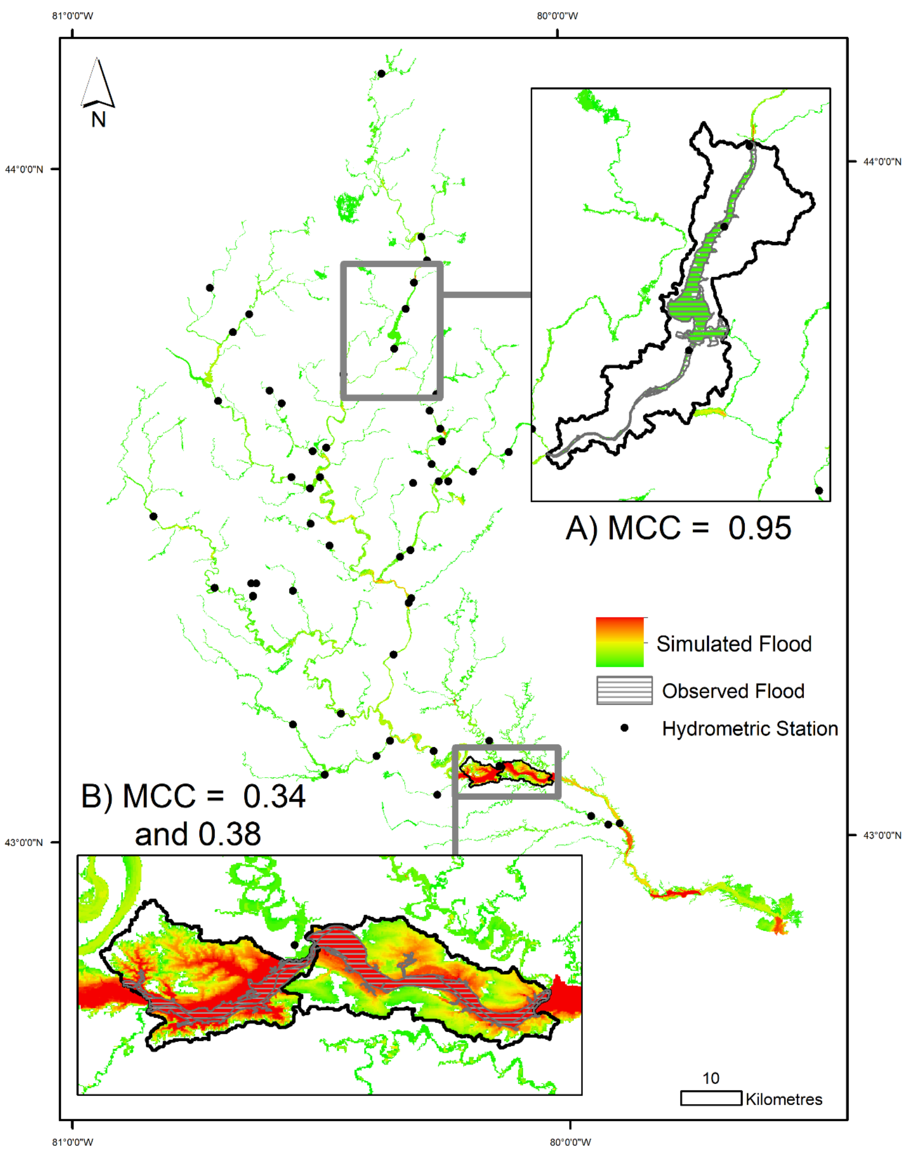

https://doi.org/10.5194/gmd-2020-316
Preprint. Discussion started: 28 October 2020

1175 Figure 12. Observed and Simulated Flood Extents– Ottawa River Watershed

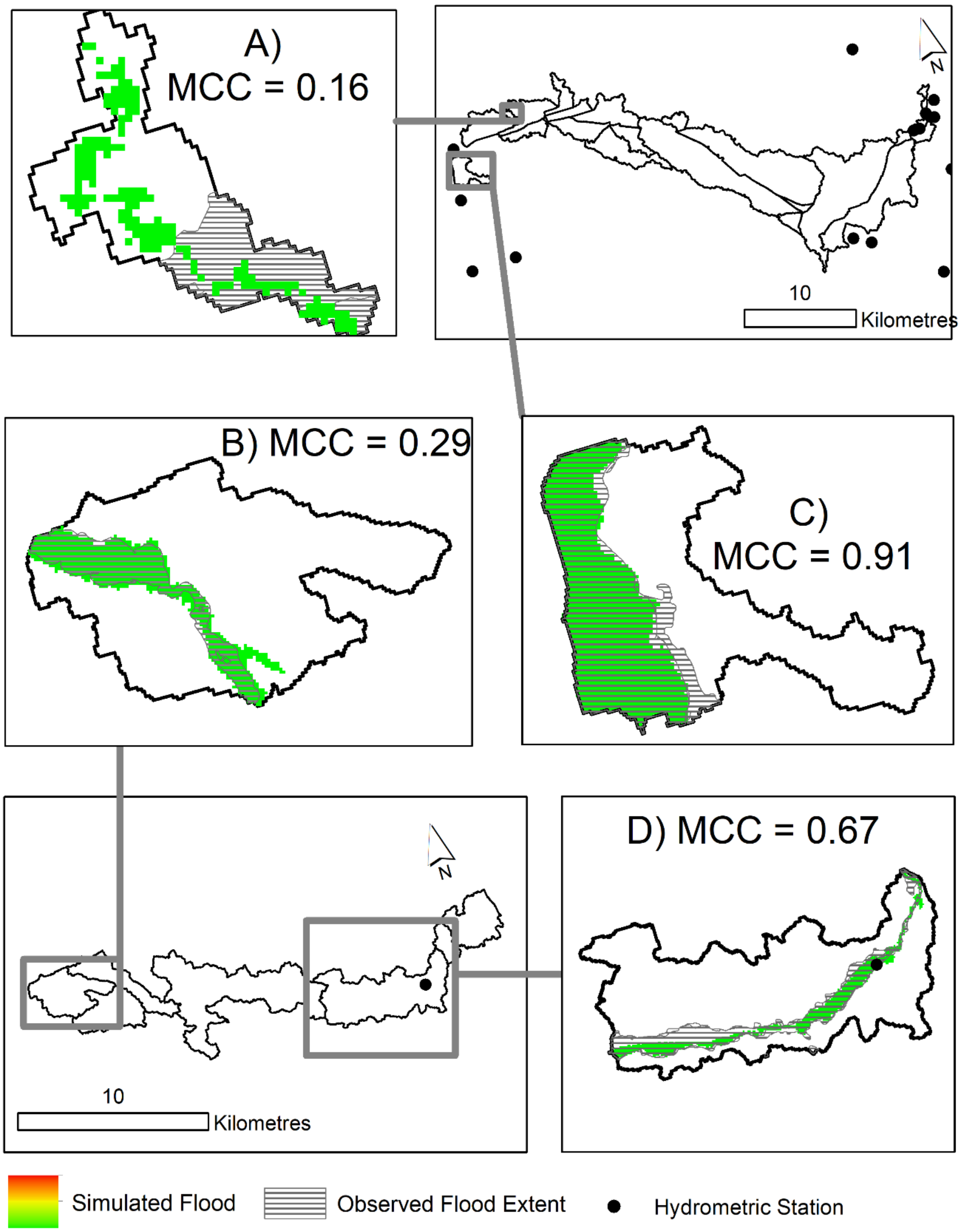

1176
1177
1178

Geoscientific Model Development Discussions
Open Access

Acknowledgement:

Thank you, Majid Hojati and Amit Kumar, for assistance in GIS and software set up.

The flood extent products are derived from satellite images and ancillary data with a system developed and operated by the Strategic Policy and Innovation Sector of Natural Resources Canada © Department of Natural Resources Canada. All rights reserved.

Data credited to the Grand River Conservation Authority contains information made available under Grand River Conservation Authority's Open Data Licence v2.0.

https://doi.org/10.5194/gmd-2020-316
Preprint. Discussion started: 28 October 2020

Geoscientific Model Development
Discussions

Funding

This work was funded by the Global Water Futures research programme under the Developing Big Data and Decision Support Systems theme.

Conflicts of interest/Competing interests

The authors declare that there are no competing interests.

Availability of data and material

Any data that support the findings of this study, not already publicly available, are available from the corresponding author, C. Chaudhuri, upon reasonable request.

Author Contribution

The idea behind this research was conceived, implemented, and written equally by all the authors.

Code availability

The current version of InnundatEd is available from the project GitHub website: https://github.com/thespatiallabatLaurier/floodapp_public. The exact version of the model used to produce the results used in this paper is archived on Zenodo (*10.5281/zenodo.4095618*).